

Peeking into the next decade in Large-Scale Structure Cosmology with its Effective Field Theory

Diogo Bragança^{1,2}, Yaniv Donath³, Leonardo Senatore⁴, and Henry Zheng^{1,2}

¹ *Stanford Institute for Theoretical Physics, Physics Department,
Stanford University, Stanford, CA 94306*

² *Kavli Institute for Particle Astrophysics and Cosmology,
SLAC and Stanford University, Menlo Park, CA 94025*

³ *Department of Applied Mathematics and Theoretical Physics,
University of Cambridge, Cambridge, CB3 0WA, UK*

⁴ *Institut für Theoretische Physik, ETH Zurich, 8093 Zurich, Switzerland*

Abstract

After the successful full-shape analyses of BOSS data using the Effective Field Theory of Large-Scale Structure, we investigate what upcoming galaxy surveys might achieve. We introduce a “perturbativity prior” that ensures that loop terms are as large as theoretically expected, which is effective in the case of a large number of EFT parameters. After validating our technique by comparison with already-performed analyses of BOSS data, we provide Fisher forecasts using the one-loop prediction for power spectrum and bispectrum for two benchmark surveys: DESI and MegaMapper. We find overall great improvements on the cosmological parameters. In particular, we find that MegaMapper (DESI) should obtain at least a 12σ (2σ) evidence for non-vanishing neutrino masses, bound the curvature Ω_k to 0.0012 (0.012), and primordial inflationary non-Gaussianities as follows: $f_{\text{NL}}^{\text{loc}}$ to ± 0.26 (3.3), $f_{\text{NL}}^{\text{eq}}$ to ± 16 (92), $f_{\text{NL}}^{\text{orth}}$ to ± 4.2 (27). Such measurements would provide much insight on the theory of Inflation. We investigate the limiting factor of shot noise and ignorance of the EFT parameters.

Contents

| | | |
|----------|--|-----------|
| 1 | Introduction and Summary | 3 |
| 2 | Technical aspects of the Fisher Matrix | 7 |
| 2.1 | Power spectrum and bispectrum | 8 |
| 2.2 | Combining redshifts | 11 |
| 2.3 | Survey specifications at different redshifts | 12 |
| 2.4 | Further ingredients from data analyses | 15 |
| 3 | Pipeline validation against BOSS data analysis | 17 |
| 3.1 | Fisher prediction against full MCMC | 18 |
| 3.2 | Fisher prediction with diagonal covariance | 20 |
| 4 | Results | 22 |
| 4.1 | BOSS | 23 |
| 4.2 | DESI | 25 |
| 4.3 | MegaMapper | 29 |
| 5 | Further constraining f_{NL} with a perturbativity prior | 31 |
| 5.1 | Contribution to the Fisher matrix | 33 |
| 5.2 | Results | 35 |
| A | Survey details and best-fits | 39 |
| B | Further analyses | 41 |
| B.1 | MegaMapper “pessimistic” results | 41 |
| B.2 | Perturbativity prior effect on base cosmological parameters | 42 |

1 Introduction and Summary

In the last few years, Large-Scale Structure (LSS) survey data have started to be analyzed using the so-called Effective Field Theory of Large-Scale Structure (EFTofLSS) [1, 2]. The approach in which the data are analyzed in the context of this theory is rather simple: all data below a certain maximum wavenumber are used in the Bayesian inference. This technique goes under the name of “full shape analysis”. Such an application to data has allowed a measurement of all cosmological parameters of the Λ CDM model using just a prior from Big Bang Nucleosynthesis [3–5]. The precision and accuracy achieved through this measurement were unexpectedly high, offering a new independent method for determining the Hubble constant with a percent-level precision [3], and for measuring Ω_m with a precision comparable to Planck [6], among other remarkable achievements. For the interested reader we provide a list of references of the application of the EFTofLSS to data in this footnote ¹. It should be stressed that the development of the EFTofLSS was a rather long journey in which the theory was developed in the various stages that are necessary to compare it to observations (dark matter, galaxies, redshift space distortions, IR-resummation, fast-evaluation techniques, MonteCarlo sampling, etc.), and along the way comparison with numerical simulations was essential to check that the theory was on the right track. Because of this, we find it fair, and also useful for the interested reader, to provide a footnote with a list of the references that were essential for the development of the EFTofLSS prior to its application to data, when it finally became clear that the approach was useful ².

¹The EFTofLSS prediction at one-loop order has been used to analyze the BOSS galaxy Power Spectrum [3–5, 7, 8], and Correlation Function [9, 10]. This was extended to eBOSS in [11]. The BOSS galaxy-clustering bispectrum monopole was analyzed in [3, 12, 13] using the EFTofLSS prediction at tree-level, and the one loop level was analyzed in [14–16]. All Λ CDM cosmological parameters have been measured from these data by only imposing a prior from Big Bang Nucleosynthesis (BBN), reaching quite a remarkable precision. For example, the present amount of matter, Ω_m , and the Hubble constant (see also [17, 18] for subsequent refinements) have error bars that are similar to the ones obtained from the Cosmic Microwave Background (CMB) [6]. For clustering and smooth quintessence models, limits on the equation of state w of dark energy of $\lesssim 5\%$ have been set using only late-time measurements [18, 19, 11], similar to the ones from CMB [6]. These measurements establish a new, CMB-independent, method for determining the Hubble constant [3], with precision comparable to one from the cosmic ladder [20, 21] and CMB. Some models that were proposed to alleviate the tension in the Hubble measurements between the CMB and cosmic ladder (see e.g. [22]) have also been compared to data [23–27]. Primordial non-Gaussianities [28, 29] and more general extended models beyond the Λ CDM universe have also been compared to BOSS data in [30–38].

²The initial formulation of the EFTofLSS was performed in Eulerian space in [1, 2], and subsequently extended to Lagrangian space in [39]. The dark matter power spectrum has been computed at one-, two- and three-loop orders in [2, 40–46, 44, 46–49]. These calculations were accompanied by some theoretical developments of the EFTofLSS, such as a careful understanding of renormalization [2, 50, 51] (including rather-subtle aspects such as lattice-running [2] and a better understanding of the velocity field [40, 52]), of several ways for extracting the value of the counterterms from simulations [2, 53], and of the non-locality in time of the EFTofLSS [40, 42, 54]. These theoretical explorations also include an enlightening study in 1+1 dimensions [53]. An IR-resummation of the long displacement fields had to be performed in order to reproduce the Baryon Acoustic Oscillation (BAO) peak, giving rise to the so-called IR-Resummed EFTofLSS [55–59]. Accounts of baryonic effects were presented in [60, 61]. The dark-matter bispectrum has been computed at one-loop in [62, 63], the one-loop trispectrum in [64], and the displacement field in [65]. The lensing power spectrum has been computed at two loops in [66]. Biased tracers, such as halos and galaxies, have been studied in the context of the EFTofLSS in [54, 67–72] (see also [73]), the

So far, the data analysis has mainly focused on the data from BOSS DR12 [87]. While there are certainly more ways in which these data can be analyzed, with many much-improved LSS surveys coming online and being designed, it is natural to ask what kind of measurement the application of the so-far developed EFTofLSS to these data will allow. In this paper, we do this by Fisher forecasting the information content of two upcoming surveys, that we take as benchmarks, DESI [88], and MegaMapper [89], including some forecasts for further analyses on BOSS. Our intention is that the results for these two upcoming and planned surveys will give an idea of the capabilities of other further surveys, either already planned or to be planned. We primarily focus on the cosmological parameters of the flat Λ CDM model, while also considering neutrino masses, curvature, and primordial non-Gaussianities (for a forecast about CDM-isocurvature modes for Euclid and MegaMapper, using just the one-loop power spectrum and tree level bispectrum, see [90]). These are in fact parameters whose detection would allow us to extend or ameliorate the standard model of cosmology and of particle physics.

For neutrinos, we know from neutrino oscillations that they are massive (see for example [91]), but we do not know the absolute value of their masses. For inflation, curvature should naturally be very small, to the order of the primordial perturbations $\sim 3 \cdot 10^{-5}$, though evidence of negative curvature could be extremely interesting, pointing towards the fact that our universe might come out of a bubble nucleation event (see for example [92] and references therein). A large positive curvature would essentially rule out eternal inflation, while a large negative curvature would rule out slow-roll eternal inflation [93]. Finally, non-Gaussianities could reveal the interaction structure of Inflation, which is actually the most insightful aspect to understand the particle physics origin of this theory. Concerning the shape of the non-Gaussianities we will explore, we will analyze the so-called $f_{\text{NL}}^{\text{loc}}$ (see e.g. [94]), $f_{\text{NL}}^{\text{eq}}$ [95] and $f_{\text{NL}}^{\text{orth}}$ [96] shapes, which parametrize a large class of non-Gaussianities that can be produced in single field inflation [97, 96], and, for $f_{\text{NL}}^{\text{loc}}$, also in multifield inflation (see e.g. [98–101]) (see also recently [102] for a forecast on MegaMapper on these parameters using just the tree-level bispectrum). It should be stressed that there exist other shapes of non-Gaussianities that are well motivated (see e.g. [103]), and we leave their exploration to future work.

Let us summarize some important technical aspects of our analysis:

- We use the prediction of the EFTofLSS at one loop order for the power spectrum and the bispectrum. We provide the Fisher forecasts by utilizing all the multipoles of the line-of-sight angle.
- The model that we implement is the same as in the analyses of the BOSS data as in [14].

In particular, this includes the integration of the one-loop bispectrum integrals as developed

halo and matter power spectra and bispectra (including all cross correlations) in [54, 68]. Redshift space distortions have been developed in [55, 74, 70]. Neutrinos have been included in the EFTofLSS in [75, 76], clustering dark energy in [77, 48, 78, 79], and primordial non-Gaussianities in [68, 80–82, 74, 83]. Faster evaluation schemes for the calculation of some of the loop integrals have been developed in [84]. Comparison with high-quality N -body simulations to show that the EFTofLSS can accurately recover the cosmological parameters have been performed in [3, 5, 85, 86].

in [104]. The modeling of primordial non-Gaussianities is done as in [28].

- We check the accuracy of our predictions against comparison with the posterior obtained by analyzing the BOSS data with the full-likelihood of [14]. We conclude that, approximately, our predictions for the error bars should be roughly accurate to about 30% or 40%, once the maximum wavenumber of the analysis has been fixed. This error is primarily influenced by our assumption of a diagonal covariance.

On top of the overall volume of the survey, we identify two limiting factors that affect the precision of the upcoming measurements. One is the discreteness of the galaxy field, which induces a shot noise term in the data, and the second is the fact that dozens of EFT parameters, including biases, need to be fitted to the observations (these EFT parameters encode the effect at long distances from uncontrolled short distance physics, which includes the relation between galaxy overdensities and matter fields). We explore these issues in the following way:

1. **Shot noise:** In addition to our main analysis, we provide Fisher forecasts with shot noise set to zero, effectively assuming an infinitely dense distribution of galaxies.
2. **EFT parameters:** We investigate the impact of limited knowledge regarding the EFT parameters by conducting Fisher forecasts in the following three ways:
 - (a) We set the width of the prior on the EFT parameters to zero, which is equivalent to fixing them. This represents the ultimate reach in terms of constraining power.
 - (b) **Galaxy Formation Prior:** We set the width of the prior on the EFT parameters to 0.3 (rather than about 2 or 4 as in the normal analyses). This is meant to represent a perhaps realistic prior on the EFT parameters as informed by astrophysical galaxy formation studies.
 - (c) **Perturbativity Prior:** Finally, we introduce a new, theoretically-justified prior on the EFT parameters that we call “perturbativity prior”, which is based on the following reasoning. In the EFTofLSS, it is possible to estimate the correct size of a loop term given the lower order terms by simple scaling formulas. It is self-consistent to impose that the loop terms in the analysis obey this estimate. If the number of parameters to fit to observations is small, this criterium is automatically satisfied once the EFT parameters have been assigned a prior of $\mathcal{O}(1)$, which is the standard way in which priors are set (see for e.g. [14]). However, when the number of parameters becomes large, say $n \gg 1$, if each parameter is $\mathcal{O}(1)$, the size of the loop can be a factor of $\mathcal{O}(\sqrt{n})$ too large, due to some random accumulation effect. It is easy to convince oneself that the data, which are most effective at the highest wavenumbers where the loop is sizable, might not provide sufficient constraining power to prevent such random accumulation effects from happening. In fact, due to cancellations among the various components of a loop term, it is possible that the loop is small at those high wavenumbers where both data and loop are strong, while the loop could still be too large at intermediate

and low wavenumbers. Indeed, at these intermediate and low wavenumbers, the data, being weaker, do not constrain the loop term, having this one become quite smaller in the meantime. We therefore set a Gaussian prior on the overall loop term, by favoring the configurations that satisfy the overall size and scaling as a function of wavenumber of the loop term. While this prior has not yet been tested on simulations or data, it is solidly theoretically justified, and we report results incorporating it.

We find the following results for DESI and MegaMapper for the various cosmological parameters:

- Ω_k : Planck 2018 constrains this parameter to 0.0065 [6]. For DESI, we forecast a constraint of about 0.051. MegaMapper instead will reduce this bound to 0.0012, representing an improvement of over 5 times compared to Planck, and just about 1.5 orders of magnitude away from the ultimate limit where it makes sense to measure this parameter, which is the amplitude of the primordial curvature fluctuation. We notice however that this bound depends quite strongly on the maximum wavenumber of the analysis.
- $\sum_i m_{\nu_i}$: Planck 2018 constrains this parameter to be <0.27 eV [6]. However, the most interesting side of the error for this parameter is the lower one, as it is associated to a detection of non vanishing masses. We find that DESI will constraint this parameter to about -0.07 eV from above the reference value (which is what is relevant for detection) with only the power spectrum (P) and -0.05 eV with the addition of the bispectrum, a significant improvement with respect to Planck. Since our bound depends on the central value of neutrino masses, a more invariant way to cast this bound is that we expect on DESI there will be a guaranteed 2σ -evidence for non vanishing neutrino masses. MegaMapper instead will reduce this bound to 0.008 eV, which should guarantee a $\gtrsim 12\sigma$ detection. After the measurement of the cosmological constant Λ , this would be the second parameter of the standard model of particle physics that is measured from cosmological observations.
- f_{NL} : Planck 2018 constraints $f_{\text{NL}}^{\text{loc.}}$ to ± 5 , $f_{\text{NL}}^{\text{eq.}}$ to ± 47 , $f_{\text{NL}}^{\text{orth.}}$ to ± 24 [105]. We find that DESI will constraint $f_{\text{NL}}^{\text{loc.}}$ to ± 3.3 , $f_{\text{NL}}^{\text{eq.}}$ to ± 92 (or ± 114 without the perturbativity prior), $f_{\text{NL}}^{\text{orth.}}$ to ± 27 , which are quite comparable to the limits obtained by Planck. MegaMapper will further reduce these bounds as $f_{\text{NL}}^{\text{loc.}}$ to ± 0.26 , $f_{\text{NL}}^{\text{eq.}}$ to ± 16 (or ± 18 without the perturbativity prior), $f_{\text{NL}}^{\text{orth.}}$ to ± 4 . These are very significant improvements with respect to Planck, that range from factors of almost three for $f_{\text{NL}}^{\text{eq.}}$, six for $f_{\text{NL}}^{\text{orth.}}$, to about a factor of 20 for $f_{\text{NL}}^{\text{loc.}}$. Such a level of improvement brings with it a clear chance of a discovery of primordial non-Gaussianities, opening the door to a deeper understanding at the particle physics level of the inflationary theory. Additionally, the allowed values for non-Gaussianities would begin to be close to that $\mathcal{O}(1)$ which represents the vague but significant threshold beyond which inflation is of the slow-roll kind.

We also study the limiting effect of shot noise and biases. We find that setting the shot noise to zero for DESI would reduce the error bars of practically all parameters by roughly a factor of

two. For MegaMapper, the reduction would be of a factor of about three for the f_{NL} ’s, and about an order of magnitude for the other cosmological parameters.

Regarding the EFT parameters, assuming perfect prior knowledge of the biases in DESI would lead to varied reductions in the error bars, typically by a factor of two. For $f_{\text{NL}}^{\text{eq}}$, the reduction would be around a factor of five. When considering our galaxy-formation benchmark prior of 0.3 instead of fixed parameters, the improvement is significantly diminished to approximately 30% for $f_{\text{NL}}^{\text{eq}}$ and $f_{\text{NL}}^{\text{orth}}$, with marginal impact on the other parameters. We find a similar behavior for MegaMapper. It appears that the perturbativity prior only captures a fraction of the potential improvement achievable through exact knowledge of the biases. It would be interesting to see if higher n -point functions or higher-order computations can improve on this.

Overall, this Fisher analysis tells us that even by just using the EFTofLSS at the current level of development, the next decade in LSS surveys could lead to great improvements in our knowledge of cosmological parameters. This includes parameters that have not yet been measured, such as neutrino masses, as well as those connected to inflation, such as primordial non-Gaussianities and the curvature of the universe. Improvements in the design of surveys to reduce shot noise, or advancements in the measurement of EFT parameters have the potential to further strengthen these already promising results.

Public Codes: The code to compute the Fisher forecasts is publicly available on GitHub ³.

2 Technical aspects of the Fisher Matrix

Fisher analyses have become a key tool for forecasting in cosmology. Pioneered in [106], there have been numerous applications over the past years (for example [107–109]). We here briefly lay out which methods we will use for our forecasts and what contributes to our estimates.

At the heart of Fisher forecasts lies the Cramér-Rao lower bound. It states that the covariance of unbiased estimators for a set of parameters θ is bounded below by the inverse of the Fisher information matrix F_{ij} , defined as the expected value of the Hessian of the log-likelihood

$$F_{ij} = -\left\langle \frac{\partial^2 \log L}{\partial \theta_i \partial \theta_j} \right\rangle. \quad (2.1)$$

Under the assumption that the likelihood is Gaussian with mean X and covariance C , we can approximately write the Fisher matrix as [106]

$$F_{ij} = \frac{\partial X^T}{\partial \theta_i} C^{-1} \frac{\partial X}{\partial \theta_j}. \quad (2.2)$$

In order to calculate the Fisher matrix, we need to assume reference parameters θ^{ref} , on which we evaluate the derivatives. In particular, the reliability of the Fisher forecast depends on this reference

³<https://github.com/YDonath/EFTofLSSFisher>

cosmology being fairly accurate. An intuitive way to see the reference cosmology dependence and also an alternative derivation for Eq. (2.2) is to start directly with a Gaussian likelihood for an observable X depending on parameters θ , that has a true mean \tilde{X} , such that the log-likelihood is given by

$$-2 \log L = (X(\theta) - \tilde{X})^T C^{-1} (X(\theta) - \tilde{X}) + p_1, \quad (2.3)$$

where p_1 is a θ -independent constant. We can then assume a reference value θ^{ref} , and Taylor expand around the reference value to first order, $X(\theta) \simeq X(\theta^{\text{ref}}) + \sum_i \frac{\partial X}{\partial \theta_i} (\theta_i - \theta_i^{\text{ref}})$. If $X(\theta^{\text{ref}})$ is accurate we can identify that the \tilde{X} term in Eq. (2.3) cancels with $X(\theta^{\text{ref}})$ ⁽⁴⁾. What remains is the first order term, which we can substitute back into Eq. (2.3), to get

$$-2 \log L = (\theta - \theta^{\text{ref}})^T F (\theta - \theta^{\text{ref}}) + p_1, \quad (2.4)$$

where we get the same formula for the Fisher matrix, F , as in Eq. (2.2). In Eq. (2.4) we can now clearly see that the Fisher matrix is the inverse covariance for the likelihood of the parameter vector θ . As can be seen from the derivation above, the Fisher formalism is sensitive to an accurate reference cosmology in order for \tilde{X} to cancel with $X(\theta^{\text{ref}})$ and also for the Taylor expansion to be an accurate approximation. Given that we now have precise measurements of all cosmological and EFT parameters [110] we have good reason to believe we are making realistic predictions around a realistic reference cosmology. In fact, we will show in Sec. 3 that we can reproduce results from previous surveys to great precision. We also checked that slight deviations from this reference cosmology do not greatly alter our results.

Note that Eq. (2.2) is in principle simply an inverse-covariance weighted sum over all available information. Both the mean and the covariance can be modeled using perturbation theory. We will discuss this in Secs. 2.1 and 2.2. Then in Sec. 2.3 we will discuss further ingredients that go into calculating the Fisher matrix, such as fixing the reference bias parameters at different redshifts. We here always refer to the correlators of galaxies in redshift space. Therefore, unless explicitly mentioned, we drop the h,r index with respect to the notation in [111], and by P, B, δ, \dots we always indicate the quantities for biased tracers in redshift space.

2.1 Power spectrum and bispectrum

For both the power spectrum and bispectrum there are well-established thin-shell averaged estimators that predict the mean and covariance for Eq. (2.2). We use the estimators that bin in the momenta, but not in the line of sight ⁵, since we have enough analytical control to integrate over the full line of sight information.

Furthermore, for both correlators, we use leading-order contributions in the covariance, in particular neglecting power spectrum-bispectrum cross-covariance. We will discuss the impact of this approximation in Sec. 3.2. This assumption in particular implies that we can write the

⁴Note that the Taylor expansion to first order is sufficient exactly because of this cancelation.

⁵Binning in line of sight angles is also possible, see for example [108].

combined power spectrum and bispectrum Fisher matrix, F^{P+B} , as the sum of the individual Fisher matrices

$$F^{P+B} = F^P + F^B, \quad (2.5)$$

where F^P and F^B are the power spectrum and bispectrum Fisher matrices respectively. Next, we will discuss these individual contributions.

Power spectrum For the power spectrum, the estimator is given by [106, 112]

$$\hat{P}(k; \hat{z}) = \frac{1}{V_S V_P(k)} \int_{\Delta B_k} d^3 q \delta(q; \hat{z}) \delta(-q; \hat{z}), \quad (2.6)$$

where we used the notation $\Delta B_k = B(0, k + \frac{\Delta k}{2}) \setminus B(0, k - \frac{\Delta k}{2})$ and $B(a, r)$ is the ball of radius r around the point a . V_S is the survey volume and $V_P(k) = 4\pi k^2 \Delta k$ is a normalization factor given by just the integral on the right-hand side of Eq. (2.6) without the prefactors and with the galaxy density contrast $\delta \rightarrow 1$, i.e. $V_P(k) = \int_{\Delta B_k} d^3 q$.

The expected value of the estimator is simply the power spectrum itself and we will evaluate it up to the one-loop order. That is

$$P = P_{\text{Tree}} + P_{1L}. \quad (2.7)$$

Here the tree and loop contributions include their respective stochastic and response terms. We use the exact same model as in [110, 111]. Then, for the covariance, we get

$$\begin{aligned} C_{PP}(k, k') &= \langle \hat{P}(k) \hat{P}(k') \rangle - \langle \hat{P}(k) \rangle \langle \hat{P}(k') \rangle \\ &= \frac{1}{V_S^2 V_P^2(k)} \int_{\Delta B_k \times \Delta B'_k} d^3 q_1 d^3 q_2 \left[\langle \delta(q_1; \hat{z}) \delta(-q_1; \hat{z}) \delta(q_2; \hat{z}) \delta(-q_2; \hat{z}) \rangle \right. \\ &\quad \left. - \langle \delta(q_1; \hat{z}) \delta(-q_1; \hat{z}) \rangle \langle \delta(q_2; \hat{z}) \delta(-q_2; \hat{z}) \rangle \right] \\ &= \frac{2}{V_S^2 V_P^2(k)} \int_{\Delta B_k \times \Delta B'_k} d^3 q_1 d^3 q_2 \langle \delta(q_1; \hat{z}) \delta(q_2; \hat{z}) \rangle \langle \delta(-q_1; \hat{z}) \delta(-q_2; \hat{z}) \rangle \\ &= \delta_{k, k'} \frac{4\pi^2}{V_S k^2 \Delta k} P_{\text{Tree}}(k; \hat{z})^2. \end{aligned} \quad (2.8)$$

Note that, schematically, we used $\langle \delta \delta \delta \delta \rangle = \langle \delta \delta \delta \delta \rangle_c + 3 \langle \delta \delta \rangle \langle \delta \delta \rangle$, where, by the subindex c , we mean the connected correlator. The connected four-point function is the trispectrum, which we neglect here. Of the three disconnected parts one cancels with the $\langle \hat{P}(k) \rangle \langle \hat{P}(k') \rangle$ term in the first line and the other two terms are the same, giving the factor of two in the third line. As mentioned, off-diagonal contributions to the above covariance are of the order of the trispectrum, and therefore similar in size to the one-loop power spectrum multiplied by a linear power spectrum. To be consistent in the perturbative order, given that we neglect the off-diagonal contributions, we also neglect loop contributions to the diagonal of the covariance. We will see in Sec. 3 that this leads

to a roughly 10% effect. Finally, by substituting the mean and covariance into Eq. (2.2) we get the power spectrum Fisher matrix

$$F_{ij}^P = \sum_k \frac{k^2 V_S}{4\pi^2 \Delta k} \int_{-1}^1 \frac{d\mu}{2} \frac{\partial P(k; \hat{z})}{\partial \theta_i} \frac{\partial P(k; \hat{z})}{\partial \theta_j} \frac{1}{(P_{\text{Tree}}(k; \hat{z}))^2}, \quad (2.9)$$

with $\mu = \hat{k} \cdot \hat{z}$ the line of sight angle.

Bispectrum For the bispectrum, we use the estimator [113, 114]

$$\hat{B}(k_1, k_2, k_3; \hat{z}) = \frac{1}{V_S V_B(k_1, k_2, k_3)} \int_{\Delta B_{k_{123}}} d^3 q_1 d^3 q_2 d^3 q_3 \delta_D(q_1 + q_2 + q_3) \delta(q_1; \hat{z}) \delta(q_2; \hat{z}) \delta(q_3; \hat{z}) \quad (2.10)$$

where we defined $\Delta B_{k_{123}} = \Delta B_{k_1} \times \Delta B_{k_2} \times \Delta B_{k_3}$. Similarly to the power spectrum discussion, the volume V_B is defined by just the above integral with $\delta \rightarrow 1$, without prefactors and is given by

$$\begin{aligned} V_B(k_1, k_2, k_3) &= \int_{\Delta B_{k_{123}}} d^3 q_1 d^3 q_2 d^3 q_3 \delta_D(q_1 + q_2 + q_3) \\ &= 8\pi^2 k_1 k_2 k_3 \Delta k_1 \Delta k_2 \Delta k_3 \beta(k_1, k_2, k_3), \end{aligned} \quad (2.11)$$

where, without loss of generality, we assume $k_3 \geq k_2 \geq k_1$ and $\beta(k_1, k_2, k_3) = 1$ unless $k_3 = k_1 + k_2$, in which case it is $\frac{1}{2}$. Again the mean of this estimator is simply the bispectrum itself, which we calculate up to the one-loop order as in [111]:

$$B = B_{\text{Tree}} + B_{1L}. \quad (2.12)$$

Again the tree and loop contributions include their respective stochastic and response terms. To leading order, the bispectrum-bispectrum covariance is given by ⁶

$$C_{BB}(k_1, k_2, k_3, k'_1, k'_2, k'_3) = \frac{(2\pi)^6}{V_S V_B(k_1, k_2, k_3)} s_B \prod_{i=1}^3 \left(\delta_{k_i, k'_i} P(k_i; \hat{z}) \right), \quad (2.13)$$

where s_B is a symmetry factor that is equal to 6 for equilateral triangles, 2 for isosceles triangles and 1 otherwise. Again, we do not consider off-diagonal contributions, which would be the connected six-point function, as well as bispectra squared and products of trispectra and power spectra. While these contributions are suppressed relative to the diagonal, they may be sizable in some cases and we therefore check this approximation with respect to covariances measured in mocks in Sec. 3. Finally, we bin equally in all k_i , so that if we plug Eq. (2.12) and Eq. (2.13) into Eq. (2.2),

⁶The derivation of the bispectrum covariance follows analogously to Eq. (2.8): we expand the six-point function into a sum of products of connected correlators, and neglect terms that are higher order. For more details, see for example [115].

we get the bispectrum Fisher matrix at fixed redshift (see Sec. 4.2 of [107] or Sec. 4.1.3 of [116] for more details):

$$F_{ij}^B = \frac{V_S}{(2\pi)^5} \sum_{(k_1, k_2, k_3)} \frac{1}{s_B} \int_{-1}^1 \int_0^{2\pi} d\mu_1 d\phi \frac{\partial B}{\partial \theta^i} \frac{\partial B}{\partial \theta^j} \prod_{i=1}^3 \left(\frac{k_i \Delta k}{P_{\text{Tree}}(k_i; \hat{z})} \right) \begin{cases} \frac{1}{2}, & \text{if } k_3 = k_1 + k_2 \\ 1, & \text{else} \end{cases}, \quad (2.14)$$

where $\mu_i(\mu_1, \phi) = \hat{k}_i \cdot \hat{z}$ are the projected momenta, and we omitted writing the arguments of B to avoid clutter. We use the same parametrization of the μ_i as for example in [110, 111].

2.2 Combining redshifts

In the previous section, we derived formulas for Fisher matrices for the power spectrum and bispectrum at a single redshift. However, for surveys that cover a range of redshifts, we need to combine the information from different redshift bins to compute the overall Fisher matrix. We will now lay out how we combine these redshifts.

Assuming that all EFT-parameters at different redshifts are uncorrelated⁷, the full Fisher matrix for a survey with a set of redshift bins can be expressed as the sum of the power spectrum Fisher matrix and the bispectrum Fisher matrix over the redshift bins

$$F_{\text{survey}} = \sum_z (F^P(z) + F^B(z)). \quad (2.15)$$

In all forecasts we consider, we split the survey into two sets of redshift bins, let us call them bin_1 and bin_2 . Let us write $F_{\text{survey}} = F_{\text{survey},1} + F_{\text{survey},2}$ and the sum in Eq. (2.15) for each of these two Fisher matrices simply runs over the redshifts in that particular set of bins (for BOSS this is, for example, LOWZ and CMASS, i.e. $\text{bin}_1 = \{z \in \text{Tab. 5} \mid z \leq 0.45\}$ and $\text{bin}_2 = \{z \in \text{Tab. 5} \mid z > 0.45\}$). A common approach is then to define effective redshifts z_{eff} , background number density $n_{b,\text{eff}}$, etc., and simply compute the $F_{\text{survey},i}$ with these values. This is a good approximation for the derivatives of the observables, given that the time dependence is largely dominated by the growth factors that have comparably weak time dependence. However, we find that this is not a very accurate estimate for the covariance⁸. To emphasize the different redshift-dependent contributions that enter the covariance, let us write the covariance from the previous sections in their full form:

$$\begin{aligned} C_{PP}(k, k'; z) &= \delta_{k,k'} \frac{4\pi^2}{V_S(z) k^2 \Delta k} \left((b_1(z) + f(z)\mu^2)^2 P_{11}(k) + \frac{c_1^{St}}{n_b(z)} \right)^2 \\ C_{BB}(k_i, k'_i; z) &= \frac{32\pi^4 s_B \prod_{i=1}^3 (\delta_{k_i, k'_i})}{V_S(z) k_1 k_2 k_3 \Delta k^3 \beta(k_1, k_2, k_3)} \prod_{i=1}^3 \left((b_1(z) + f(z)\mu_i^2)^2 P_{11}(k_i) + \frac{c_1^{St}}{n_b(z)} \right), \end{aligned} \quad (2.16)$$

⁷Note that the fact that the EFT-parameters at different redshifts are in principle correlated has been used in [110]. But given the large range of redshifts and the mild correction from correlations, we neglect this here. For BOSS, where the redshift binning is finer than for DESI and MegaMapper, and thus the correlation is stronger, this is a 15-20% effect. Therefore we assume for future surveys the impact will be negligible.

⁸Apart from the fact that $n_{b,\text{eff}}$ simply gives a very bad estimate for a realistic covariance (i.e. reproducing the measured covariance), notice also that the power spectrum and bispectrum covariances scale with different powers of n_b , and their measured effective numbers would not be the same.

where P_{11} is the linear dark matter power spectrum, c_1^{St} is the tree-level stochastic term and we abbreviated the triangle dependence on the left-hand side $k_i = \{k_1, k_2, k_3\}$. Defining effective numbers as an approximation is not appropriate for the covariance since it is very sensitive to accurate estimates of the survey volume V_S , number density n_b , and linear bias b_1 . Their numerical values are typically given by survey specifications, and vary greatly with redshift. Specifically, n_b greatly varies with redshift as it depends on the survey target selection and measurements. In contrast, the growth rate f and the linear power spectrum P_{11} have a comparably mild redshift dependence. However, in our analysis, we will nevertheless consider their redshift dependence for completeness.

To summarize, we have weak time dependence in the derivatives and strong redshift dependence in the covariance. Therefore, for $X \in \{P, B\}$ and $i \in \{1, 2\}$ we use the following approximation for the Fisher matrix of the two redshift bins:⁹

$$\begin{aligned} (F_{\text{survey},r}^X)_{ij} &= \sum_{z \in \text{bin}_r} \frac{\partial X^T(z)}{\partial \theta_i} C_{XX}^{-1}(z) \frac{\partial X(z)}{\partial \theta_j} \\ &\simeq \frac{\partial X^T(z_{\text{eff},r})}{\partial \theta_i} \left(\sum_{z \in \text{bin}_r} C_{XX}^{-1}(z) \right) \frac{\partial X(z_{\text{eff},r})}{\partial \theta_j}, \end{aligned} \quad (2.17)$$

where $z_{\text{eff},r}$ is the effective redshift for bin_r . The vector contractions in Eq. (2.17), represent the covariance weighted sum over the available information in the correlator X . For the modes, this leads to the sums over k in Eq. (2.9) and Eq. (2.14). We also sum over all redshift space information, which in the continuum limit turns into an integral over the redshift space angles in Eq. (2.9) and Eq. (2.14). The final full Fisher matrix that we use is $F_{\text{survey}} = F_{\text{survey},1}^P + F_{\text{survey},1}^B + F_{\text{survey},2}^P + F_{\text{survey},2}^B$.

2.3 Survey specifications at different redshifts

Now that we established how to combine the information from different redshifts, let us discuss what reference parameters we choose for each of these redshifts. Predictions from the EFTofLSS rely on a number of redshift and survey-dependent parameters. While these factors have been measured to great precision at low redshifts for the BOSS survey, we need to discuss how we extrapolate these results to different redshifts and surveys.

EFT parameters Let us first look at the approximate evolution of all EFT parameters entering the galaxy power spectrum and bispectrum. In particular, we analyze the time dependence of the physical (as opposed to the bare) parameters. There are at least two distinct origins of nuisance parameters in the EFTofLSS. On the one hand, we expand some functions (such as the stress tensor or the galaxy overdensity) in terms of all fields they can depend on, multiplied by

⁹Note that we can test the validity of $\sum_{z \in \text{bin}_r} C_{XX}^{-1}(z)$ as an approximation for the covariance on its own, given that we have measurements for the covariances of BOSS. We in part do this in Sec. 3.2 and Fig. 2, where we find very good agreement.

parameters. Schematically at linear order, with redshift space distortions implied, this is (see for example [111])

$$\delta(x, t) = b_1(t)\delta_{\text{dm}}(x, t) + \dots - c_1^h(t)\frac{k^2}{k_{\text{NL}}^2}\delta_{\text{dm}}(x, t) + \dots, \quad (2.18)$$

where δ_{dm} is the dark matter overdensity (note that δ without indices always denotes the overdensity of galaxies in redshift space). We will refer to these parameters as biases (this includes response terms, but not stochastic fields). The BOSS best-fit for the biases, \vec{b}_{BOSS} , has been determined in [110]. The explicit numerical values are in App. A. When fixing the reference cosmology for surveys at higher redshifts, we rescale the biases according to the estimated linear bias given in the survey specifications [88, 117]. Specifically for any new survey we set the reference value for the vector of biases $\vec{b} = \{b_1, b_2, \dots, c_1^h, c_2^h, \dots\}$ according to

$$\vec{b}^{\text{ref}} = \frac{b_1^{\text{ref}}}{b_{1,\text{BOSS}}}\vec{b}_{\text{BOSS}}. \quad (2.19)$$

Note that the b_1^{ref} in the tables of Sec. 4, App. A and [88, 117], account for different redshifts and different galaxy species. For the surveys we consider in this paper, we give the numerical values for b_1^{ref} in Tabs. 1, 2 and 3.

Contrary to biases, there are parameters coming from correlators of stochastic fields. For example, we have

$$\langle \delta(k, t)\delta(k', t) \rangle' \supset \langle \epsilon_A(k, t)\epsilon_B(k', t) \rangle' = \frac{1}{n_b} \left(c_1^{St} + c_2^{St} \frac{k^2}{k_{\text{NL}}^2} + \dots \right). \quad (2.20)$$

We will call these terms stochastic. Importantly, since they are Poisson distributed, they are constant in time. Therefore, given that we have a vector of measured values for the stochastic terms from BOSS, we could in principle use these reference values for all redshifts. However, we here make a slight correction relative to the analysis done in [110]. There, leading order stochastic terms, for example c_1^{St} , were varied freely, whereas they should be fixed to one, by definition of n_b ⁽¹⁰⁾. Therefore, for surveys other than BOSS, we fix the leading order stochastic parameters for the power spectrum and bispectrum, i.e. $c_1^{St, \text{ref}} = c_1^{(222), \text{ref}} = 1$, and we also do not take derivatives with respect to these parameters ¹¹. For all other terms in the vector of stochastic terms $\vec{c} = \{c_2^{St}, c_3^{St}, \dots\}$ we use

$$\vec{c}^{\text{ref}} = \frac{1}{c_{1,\text{BOSS}}^{St}}\vec{c}_{\text{BOSS}}, \quad (2.21)$$

where \vec{c}_{BOSS} is the vector of stochastic parameters measured for BOSS ¹². Explicit numerical values are given in App. A and for details on the specific parameters see [111].

¹⁰It is possible to have slight deviations from this condition [118], which we will study in future work.

¹¹For BOSS, we will let the leading order stochastic terms vary freely to validate our pipeline against previous data analyses in Sec. 3, i.e. there we take derivatives with respect to these parameters. Instead, when predicting further results in Sec. 4, we will keep them fixed for BOSS forecasts as well.

¹²In all forecasts for BOSS, we use \vec{c}_{BOSS} as reference values.

As a final remark, we note that we have tested the sensitivity of our results in Sec. 4 to small shifts in the reference values of EFT parameters and found that they do not significantly affect our findings. The parameters that have the greatest impact on our results are those used in the modeling of the covariance, namely b_1 and c_1^{St} . To ensure accurate predictions for future surveys, where the best-fit is yet unknown, we take b_1^{ref} directly from survey specifications and we set the reference value of c_1^{St} to one (with the exception of BOSS, as mentioned earlier).

Perturbative reach The perturbative reach of the EFTofLSS, parametrized by k_{max} , can be determined in simulations by setting a threshold for the theory systematic error. This was the approach used for example, in [110, 3, 19]. For the BOSS CMASS sample this is $k_{\text{max}} = 0.22h \text{ Mpc}^{-1}$ at one-loop order and $k_{\text{max}} = 0.1h \text{ Mpc}^{-1}$ at tree level. In the following, we will lay out how we estimate the k_{max} for a different survey at a different redshift, motivated by the method used in [3]. There, roughly, it was imposed that the signal-to-noise of the leading theoretical error should not be sizable in the k -bin containing the k_{max} (see footnote 23 in [3]). This is a good approximation, assuming that the signal-to-noise of the theoretical error only has a sizeable contribution in the highest k -bin. Here, however, we want to limit the full signal-to-noise of the theoretical error over all k -bins. The motivation for this is two-fold. First, this approach is binning independent, which is important to be consistent between surveys that have different bin sizes. Second even though the signal-to-noise of the leading theoretical error is well approximated by only considering contributions at large k since it grows very steeply with k , it leads to a slight overestimate of the k_{max} ⁽¹³⁾ since one does not consider the theoretical error at $k < k_{\text{max}} - \frac{\Delta k}{2}$. We, therefore, consider the theoretical error contribution at all scales. Furthermore, as was used in [110], we will use the same k_{max} for the power spectrum and the bispectrum, since we expect the k -reach to be the same. To summarize, this means we impose that the signal-to-noise of the theoretical error is the same in all surveys, which then defines the k_{max} through

$$\sum_{k=k_{\text{min}}}^{k_{\text{max},1}} \left(\frac{\sigma_{\text{theory},1}(k, z_1, \dots)}{\sigma_{\text{data},1}(k, z_1, \dots)} \right)^2 = \sum_{k=k_{\text{min}}}^{k_{\text{max},2}} \left(\frac{\sigma_{\text{theory},2}(k, z_2, \dots)}{\sigma_{\text{data},2}(k, z_2, \dots)} \right)^2, \quad (2.22)$$

where the sum runs over the k -bins of the respective survey, the dots represent further dependences, such as the EFT-parameter best-fit, and $\sigma_{\text{data/theory},i}$ are the respective theoretical and data errors that we will discuss next. The leading theoretical error is the next higher loop contribution, and we estimate the data error by perturbatively modeling the covariance. Let us focus on the theoretical error first. To good approximation [40] the L -th order loop scaling is given by

$$\sigma_{L\text{-Loop}}(k, z) = P_{11}(k, z) \left(\frac{k}{k_{\text{NL}}(z)} \right)^{(3+n(k,z))L}, \quad (2.23)$$

where $n(k, z)$ is the slope of the linear power spectrum around k . For the one-loop analysis, the theoretical error is, therefore, $\sigma_{\text{theory},i}(k, z_i, \dots) = \sigma_{2\text{-Loop}}(k, z_i)$. Note that in Eq. (2.22), any

¹³We note that on small redshift differences for example between CMASS and LOWZ, the two approaches produce the same results. Therefore, the estimates in [3] are accurate.

constant factor will drop out, so we only care about the scaling. Furthermore given that from the BOSS analysis we have $k_{\text{NL}}^{\text{BOSS}} = 0.7h \text{ Mpc}^{-1}$, we can get k_{NL} at different redshifts by solving

$$\int_0^{k_{\text{NL}}(z)} dq q^2 P_{11}(q, z) = \int_0^{0.7h \text{ Mpc}^{-1}} dq q^2 P_{11}(q, z = 0.57). \quad (2.24)$$

To estimate the data error we use the square root of the covariance estimate from Eq. (2.16), including the summation over redshifts, mentioned in Eq. (2.17). We average over the redshiftspace dependence, and do not consider shot noise¹⁴, that is

$$\begin{aligned} \sigma_{\text{data},i}(k) &= \left(\sum_{z \in \text{bin}_i} \int_{-1}^1 \frac{d\mu}{2} C_{PP,n_b \rightarrow \infty}^{-1}(z, \mu) \right)^{-1/2} \\ &= \frac{2\pi}{\sqrt{k^2 \Delta k}} \left(\sum_{z \in \text{bin}_i} \frac{V_S(z)}{P_{11}(k, z)^2} \int_{-1}^1 \frac{d\mu}{2} \frac{1}{(b_1(z) + f(z)\mu^2)^4} \right)^{-1/2} \\ &=: \frac{\tilde{\sigma}_{\text{data},i}(k)}{\sqrt{\Delta k}}. \end{aligned} \quad (2.25)$$

In practice, the sum over $z \in \text{bin}_i$ runs over the bins mentioned in Eq. (2.17). Furthermore, we defined $\tilde{\sigma}_{\text{data},\text{bin}_i}(k)$, since we will take the limit $\Delta k \rightarrow dk$, such that Eq. (2.22) turns into an integral with integration measure equal to dk . Then, for each survey bin with effective redshift z_{eff} , to estimate the L -th loop order k_{max}^L , we solve

$$\begin{aligned} &\int^{k_{\text{max}}^L} dk \frac{P_{11}(k, z_{\text{eff}})^2}{\tilde{\sigma}_{\text{data},i}^2(k)} \left(\frac{k}{k_{\text{NL}}(z_{\text{eff}})} \right)^{(3+n(k,z_{\text{eff}}))2(L+1)} \\ &= \int^{k_{\text{max}}^L, \text{CMASS}} dk \frac{P_{11}(k, z = 0.57)^2}{\tilde{\sigma}_{\text{data}, \text{CMASS}}^2(k)} \left(\frac{k}{0.7h \text{ Mpc}^{-1}} \right)^{(3+n(k,z=0.57))2(L+1)}. \end{aligned} \quad (2.26)$$

2.4 Further ingredients from data analyses

In principle, we now have all the ingredients to compute Fisher forecasts for a given survey. However, there are a number of aspects related to the data and the data-analysis that we want to consider here, in order to best predict future results. For one, there are priors that we put on cosmological parameters and EFT parameters. For completeness we also briefly discuss the Alcock-Paczynski(AP) effect.

Priors We impose priors on the EFT parameters that are very similar to those used in [110]. Given that we are assuming a Gaussian likelihood in the Fisher analysis, imposing a Gaussian prior amounts to adding the inverse variance of the prior to the diagonal of the Fisher matrix.

¹⁴Setting shot noise contributions in the covariance to zero gives more conservative values for k_{max} . However, in surveys with large shot noise (i.e. we underestimate k_{max} more), contributions from higher k are negligible exactly because of this large shot noise.

The key difference between the priors we have in the Fisher analysis and those in the MCMC is that all of our priors are centered around the best-fit value rather than around zero. However, we have verified that this difference has a negligible impact on the error bars. For the special case of the linear bias b_1 , we use a log-normal prior of variance 0.8 to ensure its positivity¹⁵ For all other EFT parameters, we put a Gaussian prior of width 2, except for response and stochastic terms that are joint between the power spectrum and bispectrum, for which we use a Gaussian prior of width 4. These variance choices are analogous to the ones in [110].

We anticipate or hope that, in the coming years, our understanding of galaxy formation will advance to a level that will allow for stronger priors on the EFT parameters. In parts of Secs. 4 and 5.2 we, therefore, separately use a “galaxy-formation prior”, where we put a Gaussian prior of width 0.3 on all EFT parameters, except for b_1 where we put again a log-normal prior, also with width 0.3. This value of the prior is a benchmark value we deemed reasonably close to what can be potentially achieved.

For the cosmological parameters, we use a Gaussian Big-Bang Nucleosynthesis (BBN) prior on the baryon abundance ω_b centered around the best-fit value and, with a width of $\sigma_{\text{BBN}} = 0.00036$. Also, we analyze $\log m_\nu^{\text{tot.}} := \log(\sum_i m_{\nu_i}/\text{eV})$ rather than $\sum_i m_{\nu_i}$ which implicitly ensures unbounded positivity, with support $(0, \infty)$, on the neutrino masses, since the logarithm ensures positivity¹⁶. In the results Sec. 4 we transform the predicted error on $\log m_\nu^{\text{tot.}}$ back to a 68% interval on $\sum_i m_{\nu_i}$ (¹⁷). We do not assume any previous knowledge about the other cosmological parameters. Overall, our choice of priors is almost equivalent to those used in the data analyses [110, 5].

Alcock-Paczynski effect Galaxy spectra are measured on celestial coordinates. In order to transform to cartesian coordinates, a reference cosmology needs to be assumed, that might not correspond to the true cosmology. This discrepancy between the reference cosmology and the true

¹⁵Even though the Fisher formalism only allows for Gaussians, we can put log-normal priors, by analyzing $\log(b_1)$ rather than b_1 , since the derivative with respect to $\log(b_1)$ can easily be computed. Then imposing a log-normal prior is just a Gaussian on the “log of the parameter”.

¹⁶In [5], a flat prior with, for example, width [0.06eV, 0.9eV] was used, which would slightly ameliorate the results presented here.

¹⁷Note that the Fisher forecast predicts $\sum_i m_{\nu_i} \sim \text{Lognormal}\left(\left(\log m_\nu^{\text{tot.}}\right)^{\text{ref}}, \sigma\left(\log m_\nu^{\text{tot.}}\right)^2\right)$, thus the upper and lower bounds of the 68% confidence interval can be easily computed from the lognormal distribution. However, while the confidence interval bounds for the Gaussian posterior of $\log m_\nu^{\text{tot.}}$ are independent of the reference neutrino mass (to the extent that the Fisher forecast is), the confidence interval for $\sum_i m_{\nu_i}$ derived from the Gaussian of $\log m_\nu^{\text{tot.}}$, is in fact reference value dependent. To see this, note that the p -quantile for a Gaussian is of the form $\left(\log m_\nu^{\text{tot.}}\right)^{\text{ref}} + \sigma\left(\log m_\nu^{\text{tot.}}\right)\sqrt{2}\text{erf}^{-1}(2p-1)$ whereas for the lognormal it is of the form $\sum_i m_{\nu_i}^{\text{ref}} \times \exp\left[\sigma\left(\log m_\nu^{\text{tot.}}\right)\sqrt{2}\text{erf}^{-1}(2p-1)\right]$. Therefore, if we write confidence interval bounds in the Gaussian case, of the form $\left(\log m_\nu^{\text{tot.}}\right)^{\text{ref}}_{\sigma_{\pm}}^{\sigma_{\pm}}$, the error would be $\sigma_{\pm} = \sigma\left(\log m_\nu^{\text{tot.}}\right)\sqrt{2}\text{erf}^{-1}(2p_{\pm}-1)$, so the σ_{\pm} are reference value independent (as long as $\sigma\left(\log m_\nu^{\text{tot.}}\right)$ is). In the lognormal case, i.e. errors of the form $\left(\sum_i m_{\nu_i}^{\text{ref}}\right)_{\sigma_{\pm}}^{\sigma_{\pm}}$, we instead have $\sigma_{\pm} = \sum_i m_{\nu_i}^{\text{ref}} \times \left(\exp\left[\sigma\left(\log m_\nu^{\text{tot.}}\right)\sqrt{2}\text{erf}^{-1}(2p_{\pm}-1)\right] - 1\right)$. We emphasize, therefore, that the upper and lower bounds of the confidence interval for the lognormal distribution scale linearly with the reference value. Therefore, when in Sec. 4, we present confidence intervals $[a, b]$ for $\sum_i m_{\nu_i}^{\text{ref}} = 0.1$ eV, the confidence interval for $\sum_i m_{\nu_i}^{\text{ref}} = 0.2$ eV would be $[2a, 2b]$.

cosmology introduces a geometric distortion known as the Alcock-Paczynski (AP) effect [119]. In order to account for this effect one has to evaluate the theory model on transformed wave numbers, given by

$$k = \frac{k^{\text{ref}}}{q_{\perp}} \left[1 + (\mu^{\text{ref}})^2 \left(\frac{1}{F^2} - 1 \right) \right]^{1/2}, \quad \mu = \frac{\mu^{\text{ref}}}{F} \left[1 + (\mu^{\text{ref}})^2 \left(\frac{1}{F^2} - 1 \right) \right]^{-1/2}, \quad (2.27)$$

where

$$q_{\perp} = \frac{D_A(z)h}{D_A^{\text{ref}}(z)h^{\text{ref}}}, \quad q_{\parallel} = \frac{H^{\text{ref}}(z)/h^{\text{ref}}}{H(z)/h}, \quad F = q_{\parallel}/q_{\perp}, \quad (2.28)$$

and D_A being the angular diameter distance.

Importantly, this transformation is invertible, and therefore, information preserving. Therefore, the AP effect does not lead to any addition or loss of information, when analyzing all (i.e. the full set of multipoles) information available from a given galaxy statistic at a given order. With the exception of a small part of Sec. 4.1, in Sec. 4 we will always analyze the full set of multipoles, where the AP effect is, therefore, irrelevant, and therefore we do not include it. The only forecasts where we do not analyze the full set of multipoles are in the beginning of Sec. 4.1, and Sec. 3. The relevance of the AP effect on the Fisher forecasts is thus limited to these specific analyses and we, therefore, implement only approximate formulae. The general structure of the correlators we analyze are sums of products of rational functions in k and μ , multiplying linear power spectra and loop integrals. For both cases, we use that $(\frac{1}{F^2} - 1)$ is very close to zero and we can Taylor expand it. For the rational functions, we use

$$k^n \simeq \left(\frac{k^{\text{ref}}}{q_{\perp}} \right)^n \left(1 + \frac{n}{2} (\mu^{\text{ref}})^2 \left(\frac{1}{F^2} - 1 \right) \right), \quad \mu^n \simeq \left(\frac{\mu^{\text{ref}}}{F} \right)^n \left(1 - \frac{n}{2} (\mu^{\text{ref}})^2 \left(\frac{1}{F^2} - 1 \right) \right). \quad (2.29)$$

Instead, when evaluating loop integrals or linear powers spectra, we average the k above over redshift space angles, and we, therefore, evaluate on

$$k_{\text{avg}} = \frac{k^{\text{ref}}}{q_{\perp}} \left(1 + \frac{1}{6} \left(\frac{1}{F^2} - 1 \right) \right). \quad (2.30)$$

As we will see in Sec. 3, this approximation is enough to recover large parts of the AP effect.

3 Pipeline validation against BOSS data analysis

Ultimately, the constraints derived from the Fisher formalism are an approximation to a more complicated MCMC analysis. For one, an MCMC will in general produce non-Gaussian posteriors (see Fig. 3 in [28] for an example). In addition, there are several modeling effects that are considered in the data analyses that we do not account for in our Fisher analysis. In this section, we quantify how much these unaccounted-for effects contribute to the constraints, and thereby estimate the level of precision we can have confidence in when performing Fisher forecasts.

We split this section into two parts. In Sec. 3.1, we focus on observational effects. To isolate the impact of observational effects on the posterior, we fix the covariance entering the Fisher

matrix to the one obtained from the data analysis (i.e. the measured covariance extracted from mocks as in [110]). The remaining difference is what we call observational effects, which we do not account for¹⁸. Then in Sec. 3.2 we validate the modeling of the covariance described in Sec. 2. In particular, we study the extent to which the off-diagonal entries in the covariance impact the Fisher forecast. Throughout this section, we consider the power spectrum multipoles P_ℓ for $\ell = 0, 2$ and the bispectrum monopole B_0 at 1-loop. We also focus mainly on constraints of base cosmological parameters (h , $\ln(10^{10} A_s)$ and Ω_m). We expect this to be sufficient to quantify the accuracy of the Fisher forecasts presented in Sec. 4. As mentioned in Sec. 2.3, we here vary the leading order stochastic parameters freely, since we compare to an MCMC that does not fix them either. This is in contrast to what we will do in Sec. 4.

However, let us discuss here also the validation of our results for primordial non-Gaussianity. While what we discuss in the next sections is also applicable to non-Gaussianity, we highlight here additional validations specific to non-Gaussianity. For example, while we use the best-fit of the data analysis from [110] as our reference cosmology (see App. A for details), for f_{NL} we use $f_{\text{NL}}^{\text{ref}} = 0$ (19). The observational effects that we discuss in Sec. 3.1 affect non-Gaussianity constraints minimally. Furthermore, since almost all of the information about non-Gaussianity (with the exception of $f_{\text{NL}}^{\text{loc}}$) lies in the bispectrum, the exclusion of the power spectrum bispectrum cross-correlation in the covariance is not as sizeable as for other parameters. In conclusion, we are able to estimate that our forecast for f_{NL} is accurate to roughly 10 – 25%, as we study in more detail in Sec. 3.2.

3.1 Fisher prediction against full MCMC

Even when using the same covariance, the same perturbative model, and the same reference cosmology, there are still several effects that lead to a difference between data analysis constraints and Fisher constraints. The most important observational effects are the Alcock-Paczynski(AP) effect and the smoothing effect of the window function convolution. To evaluate the significance of these effects, we perform a Fisher forecast, using the same model, best-fit, priors, covariance, bins, etc. as in [110, 111]. The sole difference is that in one case we get the posteriors through the Fisher prediction (and only considering an approximate AP effect, and not considering window functions), and in the other through an MCMC that takes these effects into account²⁰. This in particular means, we avoid most of the discussion from Sec. 2, since we are not estimating the covariance here and also do not change any of the bias parameters nor the k_{max} . We highlight, that the AP effect will eventually not affect the results of the forecasts, since we consider all multipoles and the transformation in Eq. (2.27) is information preserving. We consider it here only because the analysis we use as reference point have been done on a limited number of multipoles. The results of the MCMC against the Fisher are shown in Fig. 1.

¹⁸We call them observational effects because the error comes from neglecting window functions and only using an approximate version of the AP effect.

¹⁹We validated that non-zero background values for f_{NL} , such as the ones allowed by the BOSS data analysis [28] or Planck [105], yield very similar constraints.

²⁰As a reference point, we take the same chain of the analysis [110] (figure 1, $P_\ell + B_0^{1loop}$).

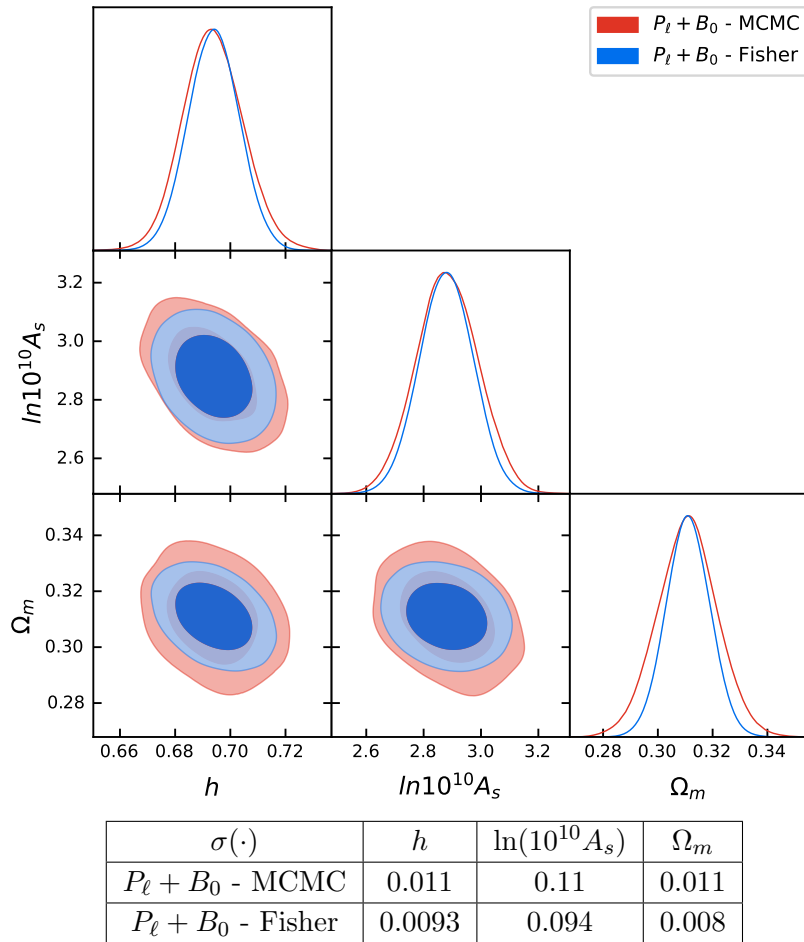


Figure 1: Triangle plots and errors comparing a Fisher forecast (blue) against the data analysis from [110] (red) for base Λ CDM parameters. For the Fisher forecast the full measured covariance is used including all cross-correlations. We here analyze $\ell = 0, 2$ power spectrum multipoles and the bispectrum monopole, both at one loop order. We implement the approximate AP effect as discussed in Sec. 2.4.

We observe that the largest discrepancy in the σ , at 27%, is found for Ω_m . However, for the other cosmological parameters, the difference is only around 15%. We expect a similar level of error, at approximately 15%, for the other parameters that we analyze in the following sections and attribute the higher discrepancy on Ω_m to not fully modelling the AP effect, which most notably depends on Ω_m . However, as argued above this effect will not be relevant for us in later sections. We note that if we remove the AP effect and window functions from the BOSS data analysis, the difference to the forecast is less than 5% ²¹.

²¹Therefore, the non-Gaussian nature of the MCMC-posteriors and the Taylor expansion around the best-fit that the Fisher relies on have minimal impact on the results.

3.2 Fisher prediction with diagonal covariance

For upcoming surveys, the fully measured covariance from mocks is not readily available. Although it is possible to compute these covariances with high accuracy using perturbation theory, the modeling of off-diagonal contributions can be very complex. Therefore, as described in Sec. 2, we do not consider any off-diagonal contributions here ²². Explicitly this means we neglect cross-correlations between the power spectrum and bispectrum and also we neglect cross-correlations between k -bins (for the power spectrum and bispectrum respectively) ²³.

By considering the diagonal elements of the measured covariance (actively putting the off-diagonal elements to zero), we can study two effects. First, we can better understand the contribution of off-diagonal elements to the covariance, without yet relying on perturbation theory. Secondly, we can investigate the precision of the analytical diagonal covariance as described in Sec. 2 by comparing them to the diagonals of the measured covariance.

The most significant effect of using a diagonal covariance is an overestimation of the bispectrum impact relative to the power spectrum. We find that the off-diagonal elements in the power spectrum covariance have a negligible effect. However, for the bispectrum, the impact is larger. This is expected, as neglecting the power spectrum-bispectrum cross-correlation is equivalent to a scenario where the bispectrum is providing purely independent, new, information from the power spectrum. At least on large enough scales, this is inaccurate as discussed in [115]. In that sense, neglecting the cross-covariance is a double counting of large-scale information. Keeping this in mind, we still want to emphasize that the relative impact of the bispectrum grows rapidly with higher k_{max} .

In Fig. 2, we show the impact of these two isolated effects. First, by reducing the full covariance to just the diagonals, we obtain about 25% – 30% tighter constraints. Second, if we compare the measured diagonal covariance to the modeled one, the agreement is remarkably good with only a few percent difference ²⁴. In fact, this could be accounted for by loop order contributions that we did not consider in our analytic modeling of the diagonal covariance which is roughly of the same order.

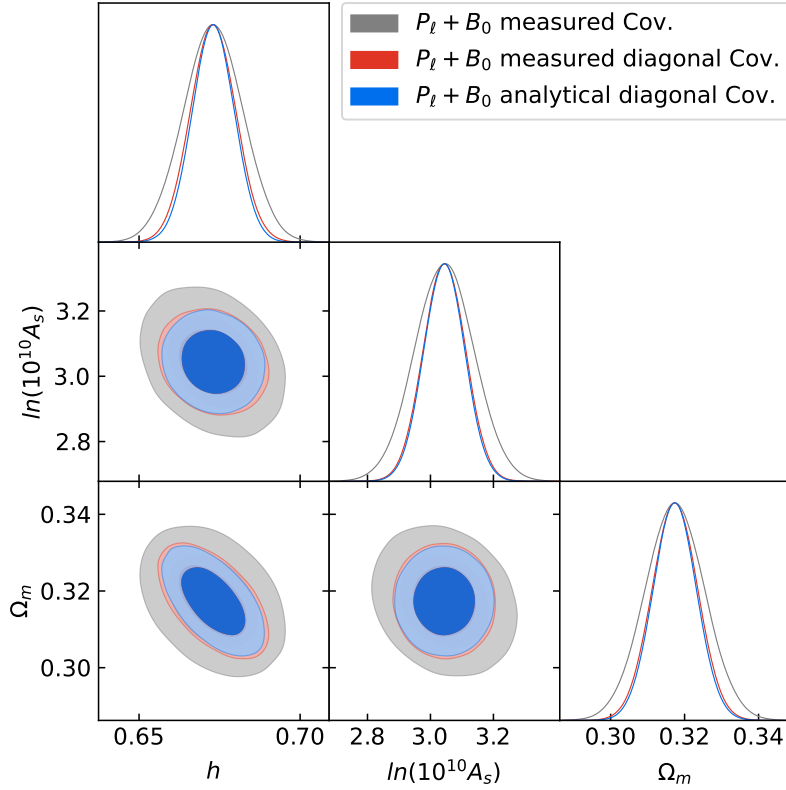
By comparing the MCMC data analysis in Fig. 1 to the Fisher forecast using the analytical diagonal covariance shown in Fig. 2, we estimate our confidence in the Fisher results to be about 40%.

Finally, we perform the same comparison for non-Gaussianity constraints. The MCMC data analysis yields $(\sigma(f_{\text{NL}}^{\text{loc.}}), \sigma(f_{\text{NL}}^{\text{eq.}}), \sigma(f_{\text{NL}}^{\text{orth.}})) = (35, 298, 75)$, while the Fisher forecast with analytical diagonal covariance gives $(\sigma(f_{\text{NL}}^{\text{loc.}}), \sigma(f_{\text{NL}}^{\text{eq.}}), \sigma(f_{\text{NL}}^{\text{orth.}})) = (28, 275, 95)$. Thus for non-Gaussianity, we have a much closer agreement at around 10 – 25%.

²²However, whenever we analyze multipoles, we do consider multipole cross-correlations, which in multipole space appear as off-diagonal entries. In particular, we consider the P_0 - P_2 cross-correlation.

²³We also neglect any sky correlations since it is a comparably small effect.

²⁴This strong agreement is present only when summing the different redshifts as described in Eq. (2.17) and footnote ⁹. In contrast, the agreement is not as good if we summarize the survey information to an effective redshift bin.



| $\sigma(\cdot)$ | h | $\ln(10^{10} A_s)$ | Ω_m |
|---|--------|--------------------|------------|
| $P_\ell + B_0$ measured Cov. | 0.0093 | 0.094 | 0.008 |
| $P_\ell + B_0$ measured diagonal Cov. | 0.0070 | 0.066 | 0.0061 |
| $P_\ell + B_0$ analytical diagonal Cov. | 0.0065 | 0.064 | 0.0059 |

Figure 2: Triangle plots comparing different Fisher forecasts for base Λ CDM parameters using the $\ell = 0, 2$ power spectrum multipoles and the bispectrum monopole, all at one loop order. The plots differ only in their covariances, where we compare the measured covariance (grey) including all cross-covariances, the diagonal of the measured covariance (red), and the analytical prediction for the diagonal covariance (blue). We implement the approximate AP effect as discussed in Sec. 2.4.

4 Results

Having validated the Fisher methodology with BOSS data analysis results in Sec. 3, we now use it to predict the constraining power of DESI and MegaMapper, as well as to provide some additional results for BOSS. As discussed in the previous section, due to observational effects and covariance modeling, we expect the accuracy of cosmological parameter constraints to be roughly 40%, and the non-Gaussianity parameters to be accurate to 10 – 25%.

While BOSS has now been extensively analyzed, there are still some unexplored questions, which we aim to address here. The full set of cosmological parameters we study in various combinations is $\{h, \ln(10^{10} A_s), \Omega_m, n_s, \Omega_k, \log m_\nu^{\text{tot.}}, f_{\text{NL}}^{\text{loc.}}, f_{\text{NL}}^{\text{eq.}}, f_{\text{NL}}^{\text{orth.}}\}$, where we defined $\log m_\nu^{\text{tot.}} := \log(\sum_i m_{\nu_i}/\text{eV})$. We refer to any subset of the first six parameters in this list (i.e. the list without the non-Gaussianity parameters) as “base” parameters. Throughout this section, we use the power spectrum and bispectrum of galaxies in redshift space at 1-loop order. For future surveys like DESI and MegaMapper, we use the full set of multipoles²⁵, and for BOSS we use either the full set of multipoles or the monopole and quadrupole for the power spectrum and the monopole for the bispectrum²⁶. Furthermore, following the discussion in Sec. 2.3, we fix the leading stochastic terms to one, throughout this section. Therefore, the results we will find for BOSS in this section are slightly tighter than what we presented in Sec. 3. When quoting results for primordial non-Gaussianity, we fix the cosmological parameters, as we will discuss more later this has almost always a negligible effect on our results. Finally, we note that we use fixed relationships from [28, 120] between the non-Gaussianity bias parameters $b_i^{f_{\text{NL}}}$ and galaxy bias parameters b_i , which we checked to be a negligible approximation with respect to putting an order one prior centered on $b_i^{f_{\text{NL},\text{ref}}}$ on $b_i^{f_{\text{NL}}}$ and then let it vary freely²⁷.

²⁵As we will see for the BOSS survey, using the full set of multipoles is roughly equivalent to just using the monopole and quadrupole for both the power spectrum and bispectrum.

²⁶When analyzing a finite number of multipoles, we implement the approximate AP effect as discussed in Sec. 2.4. However, when we use the complete set of multipoles, in particular for DESI and MegaMapper, the AP effect is irrelevant

²⁷Note that for $f_{\text{NL}}^{\text{ref}} = 0$, which is what we use here, in the context of the Fisher forecast, this is not even an approximation, but exact. However, even for non-zero reference values, the change in the error-bar due to this approximation can be quite well understood. If we were only to analyse the power spectrum, we would only constrain the joint parameter $b_1^{f_{\text{NL}}} f_{\text{NL}}$ rather than the individual parameters. With the inclusion of the bispectrum this degeneracy is broken due to the presence of $b_2^{f_{\text{NL}}} f_{\text{NL}}$, $b_1 f_{\text{NL}}$, and f_{NL} on its own. The only relevant parameter in the context of this discussion is $f_{\text{NL}}^{\text{loc.}}$, since for $f_{\text{NL}}^{\text{eq.}}$ and $f_{\text{NL}}^{\text{orth.}}$ almost all information lies in the bispectrum, and we also verified explicitly that the approximation is negligible. In contrast a large part of the constraint on $f_{\text{NL}}^{\text{loc.}}$ comes from the power spectrum, where however, we can easily understand the shift in error bar. Simple error propagation tells us that the error we obtain from the power spectrum with fixed $b_1^{f_{\text{NL}}}$ or with the order one prior on $b_1^{f_{\text{NL}}}$ are related to each other by

$$\sigma\left(f_{\text{NL}}^{\text{loc.,full}}\right) \simeq \sqrt{\sigma\left(f_{\text{NL}}^{\text{loc.,approx.}}\right)^2 + \sigma\left(b_1^{f_{\text{NL}}}\right)^2 \frac{\left(f_{\text{NL}}^{\text{loc.,ref}}\right)^2}{\left(b_1^{f_{\text{NL},\text{ref}}}\right)^2}}, \quad (4.1)$$

where we note that $\sigma\left(b_1^{f_{\text{NL}}}\right)$ is dominated by the prior width. Therefore these changes in the error bar are relevant,

4.1 BOSS

Base cosmological results with the one-loop power spectrum for BOSS have been presented in [3–5], neutrinos have also been analyzed in [5] and dark energy models in [19]. The combination of the power spectrum and bispectrum has led to the measurement of h , $\ln(10^{10} A_s)$ and Ω_m in [110], with the non-Gaussian parameter f_{NL} being reported in [28] and at tree level in [29, 34]. In this section, we present forecasts for the power spectrum and bispectrum with the inclusion of the sum of neutrino masses $\sum_i m_{\nu_i}$, spectral tilt n_s and spatial curvature Ω_k . We also investigate the impact of shot noise and of the EFT parameters and explore the information contained in higher multipoles. The exact numerical values of the EFT parameters, survey specification and reference cosmology that we use here and in Sec. 5 are given in App. A. Following the binning scheme used in [87], we divide the sample into two redshift bins. We use the same values of k_{NL} and b_1 for both bins since the redshift difference of the bins is very small. The effective numbers we use are summarized in Tab. 1.

| BOSS: | z_{eff} | $n_{b,\text{eff}}[(h \text{ Mpc}^{-1})^3]$ | b_1^{ref} | $(k_{\text{max}}^{\text{Tree}}, k_{\text{max}}^{1L}, k_{\text{NL}}) [h \text{ Mpc}^{-1}]$ | N_{bins}^{1L} | N_{Δ}^{Tree} | N_{Δ}^{1L} |
|-------|------------------|--|--------------------|---|------------------------|----------------------------|-------------------|
| Bin 1 | 0.32 | 2.9×10^{-3} | 1.9 | (0.09, 0.20, 0.7) | 18 | 9 | 62 |
| Bin 2 | 0.57 | 2.5×10^{-3} | 1.9 | (0.10, 0.22, 0.7) | 21 | 17 | 150 |

Table 1: BOSS effective survey specifications, calculated according to the formulas in Sec. 2 and Tab. 5 in App. A. $n_{b,\text{eff}}$ is the background galaxy number density entering the derivatives (not the covariance), N_{bins} is the number of k -bins we consider for the power spectrum and N_{Δ} is the number of triangles we consider for the bispectrum.

This section is divided into two parts, based on the type of covariance used. In the first part, we present results using the full measured covariance obtained in [110], which includes all cross-correlations. This implies that we expect our results to be accurate to about 15% (and 27% for Ω_m) as described in Sec. 3.1. In the second part, we investigate the impacts of shot noise and higher multipoles using a modeled covariance, as described in Sec. 3.2. This allows us to have better analytical control, for example in order to analyze the shot noise influence on the results.

Additional results: n_s , $\sum_i m_{\nu_i}$ and Ω_k We present the BOSS forecasts using the power spectrum monopole and quadrupole, as well as the bispectrum monopole, both at one loop order, for parameters that have previously only been analyzed with only the power spectrum (and in some cases with the tree-level bispectrum [3]). The results are summarized in Fig. 3.

if $f_{\text{NL}}^{\text{loc.,approx.}}$ and $b_1^{f_{\text{NL}}}$ have similar signal to noise $\frac{\sigma(f_{\text{NL}}^{\text{loc.,approx.}})}{f_{\text{NL}}^{\text{loc.,ref}}} \simeq \frac{\sigma(b_1^{f_{\text{NL}}})}{b_1^{f_{\text{NL},\text{ref}}}}$. For instance with quite large $f_{\text{NL}}^{\text{loc.,ref}}$ both sides of this ratio can roughly be equal to one, as was found in [28]. To be precise, using Planck constraints $f_{\text{NL}}^{\text{loc.}} = -0.9 \pm 5.1$ and a prior $\sigma(b_1^{f_{\text{NL}}}) = 2$, we find the full change in error bar for $f_{\text{NL}}^{\text{loc.}}$ with inclusion of both power spectrum and bispectrum at $f_{\text{NL}}^{\text{loc.,ref}} = -0.9$ to be 0.01%, 5%, 15% for BOSS, DESI and MegaMapper respectively, and even at the Planck $1\text{-}\sigma$ level $f_{\text{NL}}^{\text{loc.,ref}} = -6$, we find changes of 0.5%, 47%, 54%. Given in particular that what is important is a detection of non-vanishing $f_{\text{NL}}^{\text{loc.}}$, and within order one the actual value of $f_{\text{NL}}^{\text{loc.}}$ is much less important, we conclude that our forecasts are robust even when the $b_i^{f_{\text{NL}}}$ are free EFT parameters.

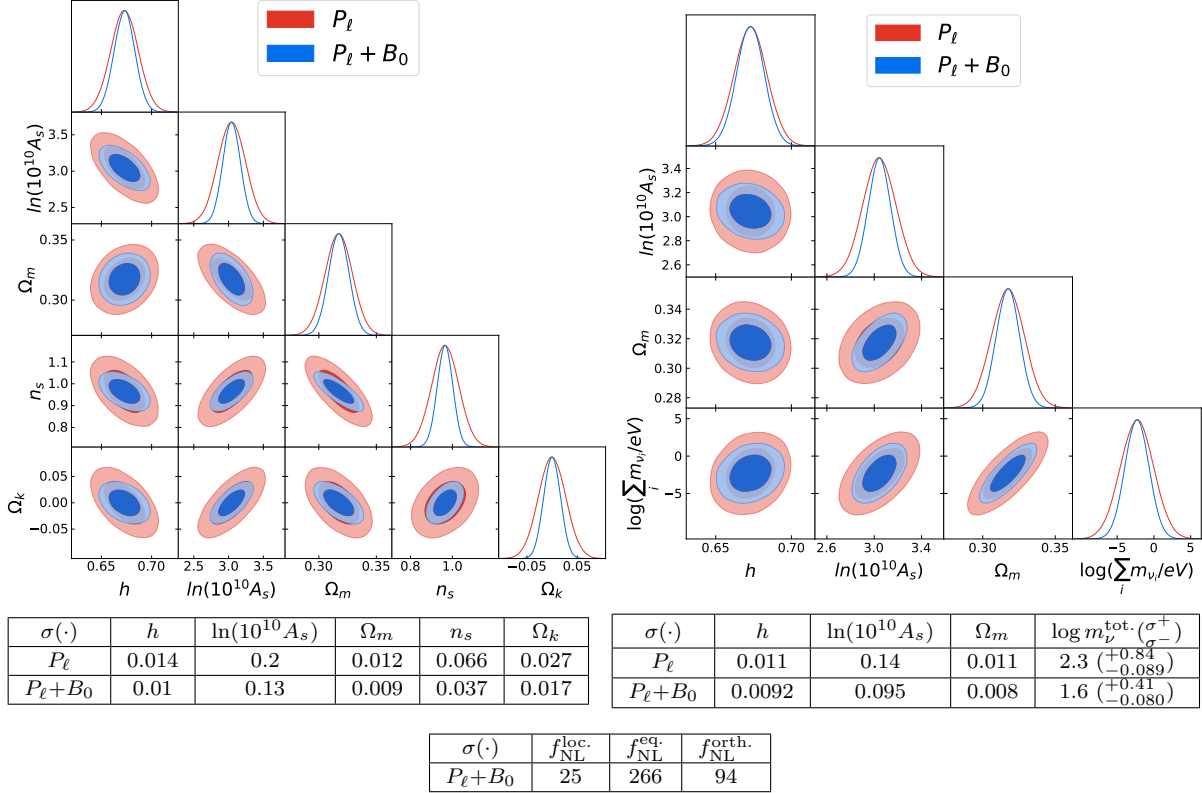


Figure 3: Triangle plots and errors from Fisher forecasts for BOSS including the spectral tilt and spatial curvature (left), massive neutrinos (right), and primordial non-Gaussianity (bottom). The power spectrum monopole and quadrupole, and the bispectrum monopole were used both at one loop order. In the table we also report the upper and lower bounds of the 68% confidence interval for the sum of massive neutrinos, i.e $\mathbb{P}[(\sum_i m_{\nu_i} - \sum_i m_{\nu_i}^{\text{ref}}) \in (\sigma^-, \sigma^+)] = 0.68$. The covariance used here is the full, measured covariance with all cross-correlations. We implemented the approximate AP effect as discussed in Sec. 2.4.

Impact of shot noise, biases and multipoles For BOSS, we checked that adding the trispectrum at tree level and the 2-loop power spectrum²⁸ do not improve on the measurements²⁹. This is mostly attributable to the large shot noise of the survey. However, given the power of the Fisher formalism, we can investigate the effects of certain limits and configurations on parameter constraints. Of course, we here look at limiting cases, that are unrealistic in reality, but they show where information is lost. In particular, we are interested in the impact of EFT parameters and of the survey shot noise. Throughout this section, we will be using the analytical covariance, which gives us the most control but comes with the caveats mentioned in Sec. 3. We investigate several effects on both base cosmological parameters including n_s , and f_{NL} . Just as in [28], unless mentioned otherwise, we fix the cosmological parameters when quoting errors on f_{NL} . We checked

²⁸While currently, we do not have the 2-loop power spectrum for galaxies in redshift space, we can simply run a Fisher analysis on the one loop correlators, with the 2-loop k_{max} reach. This then gives an upper bound estimate for the extra constraining power of the 2-loop correlators. The results on BOSS do not improve even with this optimal estimate, and therefore we believe, a 2-loop analysis will not improve the results on BOSS.

²⁹Exploration of the contribution from higher N -point functions is currently in progress [121].

that while $f_{\text{NL}}^{\text{loc.}}$ has a roughly 35% error bar reduction due to fixed cosmological parameters, $f_{\text{NL}}^{\text{eq.}}$ and $f_{\text{NL}}^{\text{orth.}}$ are very independent of the other cosmological parameters and their results would only change by roughly 5 – 10% if we would not fix the cosmological parameters.

First, we check the impact of using higher multipoles at one loop as opposed to using only the power spectrum monopole and quadrupole and the bispectrum monopole. While there is some improvement with the inclusion of additional multipoles for the bispectrum, we checked that almost all of this improvement comes from the bispectrum quadrupoles. Still, this improvement is very small, and so we do not present the posteriors. The numerical values can be found in the table of Fig. 4. We can conclude that using the monopole and quadrupole for both the power spectrum and bispectrum, one can extract almost the full redshift space information. As was shown in [110, 28], we can already analyze data with the monopole and quadrupole for the power spectrum and bispectrum. Therefore, unless indicated otherwise we analyze using all multipoles.

Next in Fig. 4, we show additional constraints in the continuous field limit $n_b \rightarrow \infty$, i.e. having no shot noise. We roughly halve the error bars for both the base cosmological parameters and f_{NL} . This should serve as motivation to include as many objects into our data sets even if they are faint or somewhat unresolved. This will also become important in Sec. 4.3.

Lastly, the EFTofLSS, like any EFT, will need a larger number of parameters when going to higher perturbative orders. This is in principle not a problem as long as they are independent enough from the parameters of interest. It is interesting to investigate how better knowledge of these parameters would impact the results. We put the “galaxy-formation prior” mentioned in Sec. 2.4, where we put stronger priors on all EFT parameters motivated by hopefully-realistic future knowledge on galaxy formation. We also take the limit in which these parameters are fixed, in other words representing the scenario in which all “nuisance” parameters are known and measured exactly with no error. This, in a sense, is the theoretical upper bound for the EFTofLSS at a given order. It is interesting to note from the results presented in the table in Fig. 4 that the biases have varying impacts on different cosmological parameters. Specifically, the biases overwhelmingly affect the primordial parameters, A_s, n_s and f_{NL} . As we will see in Sec. 5, f_{NL} -constraints are more sensitive to the EFT parameters than A_s and n_s . This is not so surprising, considering that the functional form of EFT counterterms resemble the functional form induced by primordial non-Gaussianities.

4.2 DESI

We now turn to predict the performance of upcoming surveys, starting with the imminent DESI survey. We base our results on the Emission Line Galaxies (ELGs) sample, which is the largest of the DESI surveys [88]. We note that while we are able to derive the value for the linear bias through specifications given in [88], we do not have values for the other EFT parameters. We therefore shift all biases according to the method described in Sec. 2.3, i.e. we shift them all according to the change in the linear bias with respect to the BOSS best-fit. The final numerical values we use for the DESI forecast are given in Tab. 2. For all the future surveys we use $k_{\text{min}} = 0.001h \text{ Mpc}^{-1}$ for the power spectrum and $k_{\text{min}} = 0.02h \text{ Mpc}^{-1}$ for the bispectrum. We bin with $\Delta k = 0.005h \text{ Mpc}^{-1}$ for

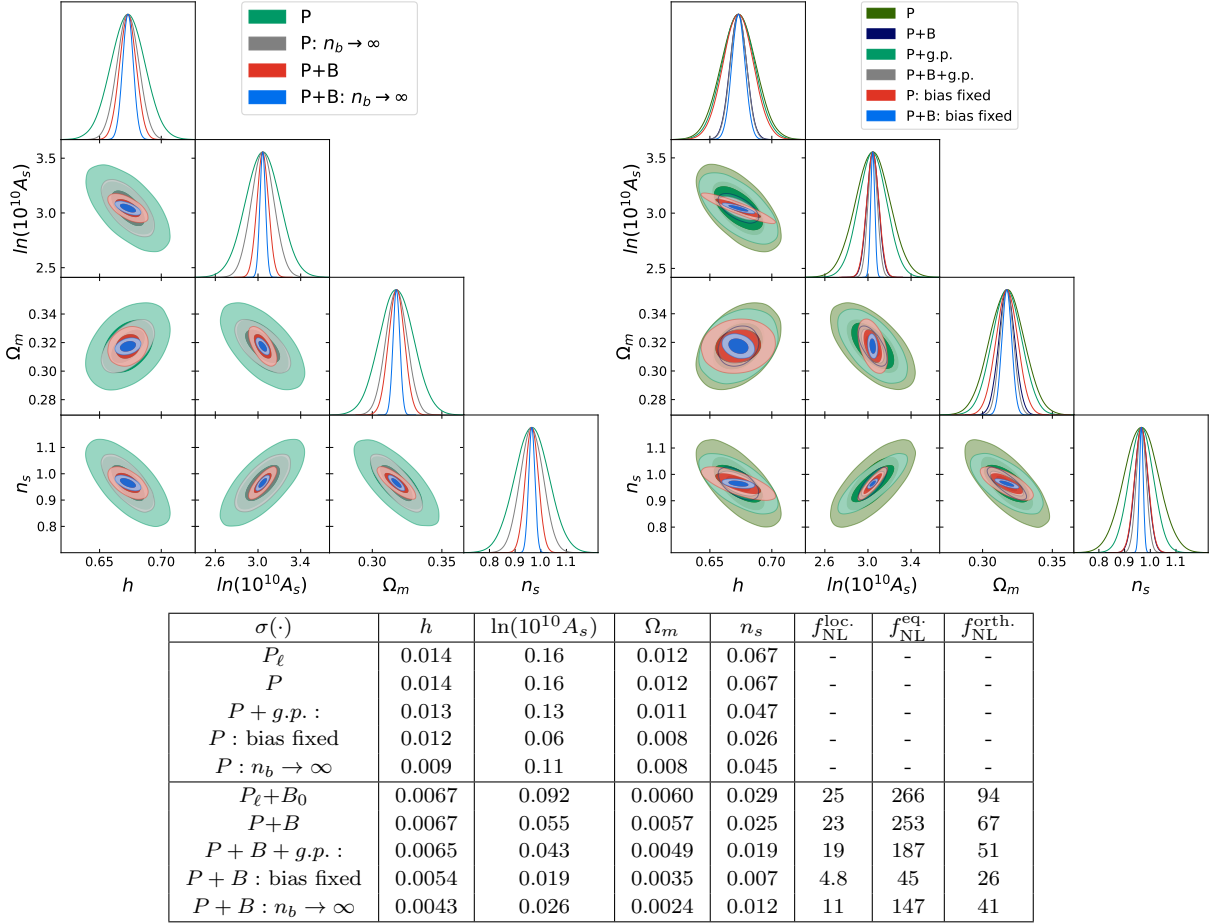


Figure 4: Triangle plots and errors from several different Fisher forecasts for BOSS using the analytical covariance. We compare base results to results obtained without shot noise (left) and with biases fixed or with a “galaxy-formation prior” (g.p.) (right). In the table, we also show the impact of including higher multipoles on the power spectrum and bispectrum and also see the impact on f_{NL} . For the constraints on f_{NL} , we fix the other cosmological parameters.

the power spectrum and $\Delta k = 0.02h \text{ Mpc}^{-1}$ for the bispectrum. For binning consistency, we have checked that using a smaller binning does not affect our results. To reduce binning effects, ideally one would always average the observables over a k -bin. However, given the numerical complexity of doing such a procedure for every bin, especially for the bispectrum, we instead evaluate on a effective number k_{eff} to approximate this averaging. This is analogous to the method used for example in [110], with the difference that we also evaluate on k_{eff} the tree level contribution, rather than averaging it. The effect is minimal. Throughout this section, we use the analytical covariance from Eq. (2.16) and Eq. (2.17) with all the ingredients discussed in Sec. 2.3. We remind that the validity of the covariance was discussed in Sec. 3.

Results We present results, including the spectral tilt, spatial curvature, neutrino masses, and non-Gaussianity in Fig. 5, using all multipoles. The results for f_{NL} were obtained with fixed

| DESI: | z_{eff} | $n_{b,\text{eff}}[(h \text{ Mpc}^{-1})^3]$ | b_1^{ref} | $(k_{\text{max}}^{\text{Tree}}, k_{\text{max}}^{1L}, k_{\text{NL}}) [h \text{ Mpc}^{-1}]$ | N_{bins}^{1L} | N_{Δ}^{Tree} | N_{Δ}^{1L} |
|-------|------------------|--|--------------------|---|------------------------|----------------------------|-------------------|
| Bin 1 | 0.84 | 8.0×10^{-4} | 1.3 | (0.08, 0.18, 0.9) | 37 | 17 | 115 |
| Bin 2 | 1.23 | 3.2×10^{-4} | 1.5 | (0.09, 0.23, 1.3) | 45 | 17 | 191 |

Table 2: DESI effective survey specifications, calculated according to the formulas in Sec. 2 and Tab. 6 in App. A. $n_{b,\text{eff}}$ is the background galaxy number density entering the derivatives (not the covariance), N_{bins} is the number of k -bins we consider for the power spectrum and N_{Δ} is the number of triangles we consider for the bispectrum.

cosmological parameters. Analyzing f_{NL} in combination with cosmological parameters changes the f_{NL} constraints by less than 8%. For neutrino masses, with the caveats discussed in footnote 17, it seems likely that DESI is already able to detect massive neutrinos at the 2σ level.

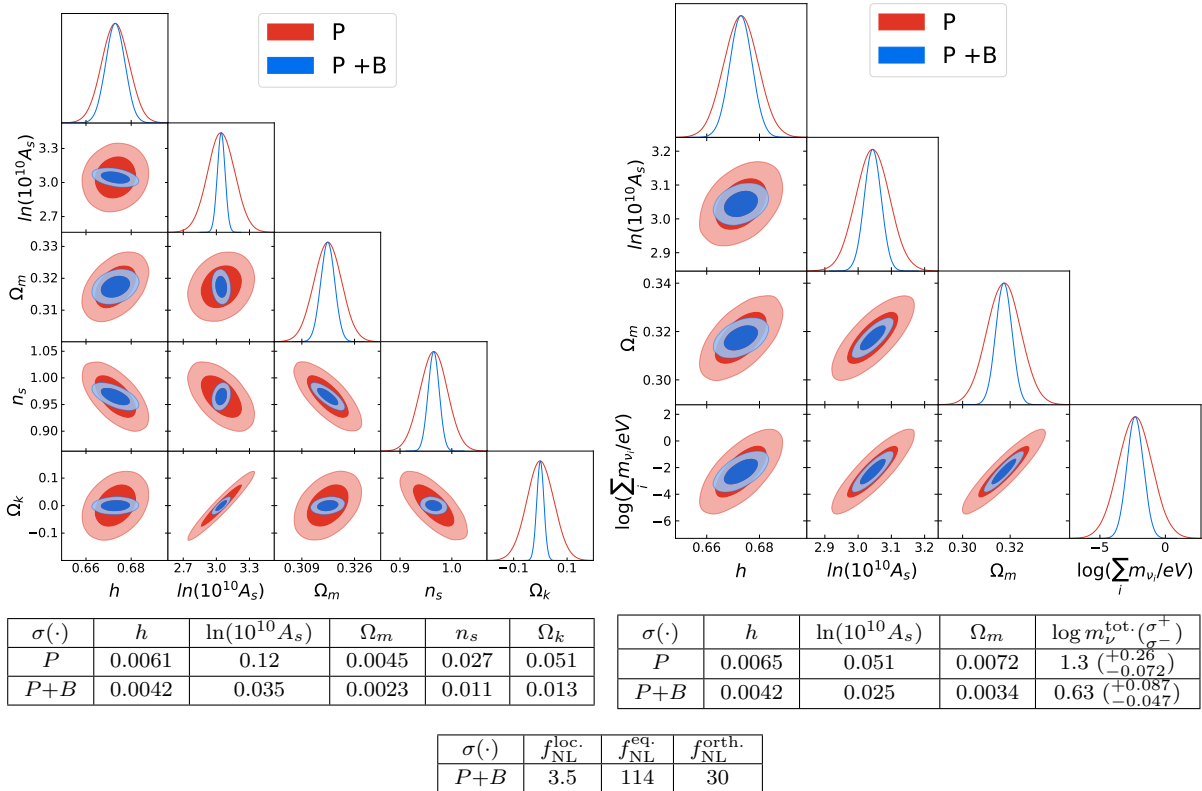


Figure 5: Triangle plots and errors from Fisher forecasts for DESI including the spectral tilt and spatial curvature (left) and massive neutrinos (right) and Non-Gaussianity (bottom). In the table we also report the upper and lower bounds of the 68% confidence interval for the sum of massive neutrinos, i.e $\mathbb{P}[(\sum_i m_{\nu_i} - \sum_i m_{\nu_i}^{\text{ref}}) \in (\sigma^-, \sigma^+)] = 0.68$. We use all power spectrum and bispectrum multipoles at one loop order for the above results and use the analytical covariance without cross-correlations.

Impact of shot noise and biases Similar to Sec. 4.1, it is interesting to investigate constraints with the “galaxy-formation prior” (g.p.) putting stronger priors on EFT parameters, and look at the theoretical limits of fixed biases and zero shot noise for DESI. As shown in Fig. 6, the

g.p. mostly affects $f_{\text{NL}}^{\text{eq.}}$ and $f_{\text{NL}}^{\text{orth.}}$. However, in both the zero shot noise ³⁰ and fixed bias limits, we observe improvements of roughly a factor of 2-3 in $\ln(10^{10}A_s)$, Ω_m and n_s , while h improves less significantly in either of these limits. These results are consistent with those obtained for BOSS in Sec. 4.1 since, as we noted, the biases have larger degeneracies with $\ln(10^{10}A_s)$, n_s , and non-Gaussianities. We find that the effect of shot noise accounts for approximately 50% of the constraints on f_{NL} . Interestingly, fixing the bias parameters has a striking effect on non-Gaussianities, particularly for $f_{\text{NL}}^{\text{eq.}}$, for which we would obtain a six-fold reduction in the error bars. In combination with the results from the g.p., this strongly motivates the need for tighter priors and therefore better measurements of biases when performing the analysis of DESI in the near future. In order to further improve on this aspect, we present in Sec. 5 the f_{NL} constraints forecasted with the EFT-motivated perturbativity prior.

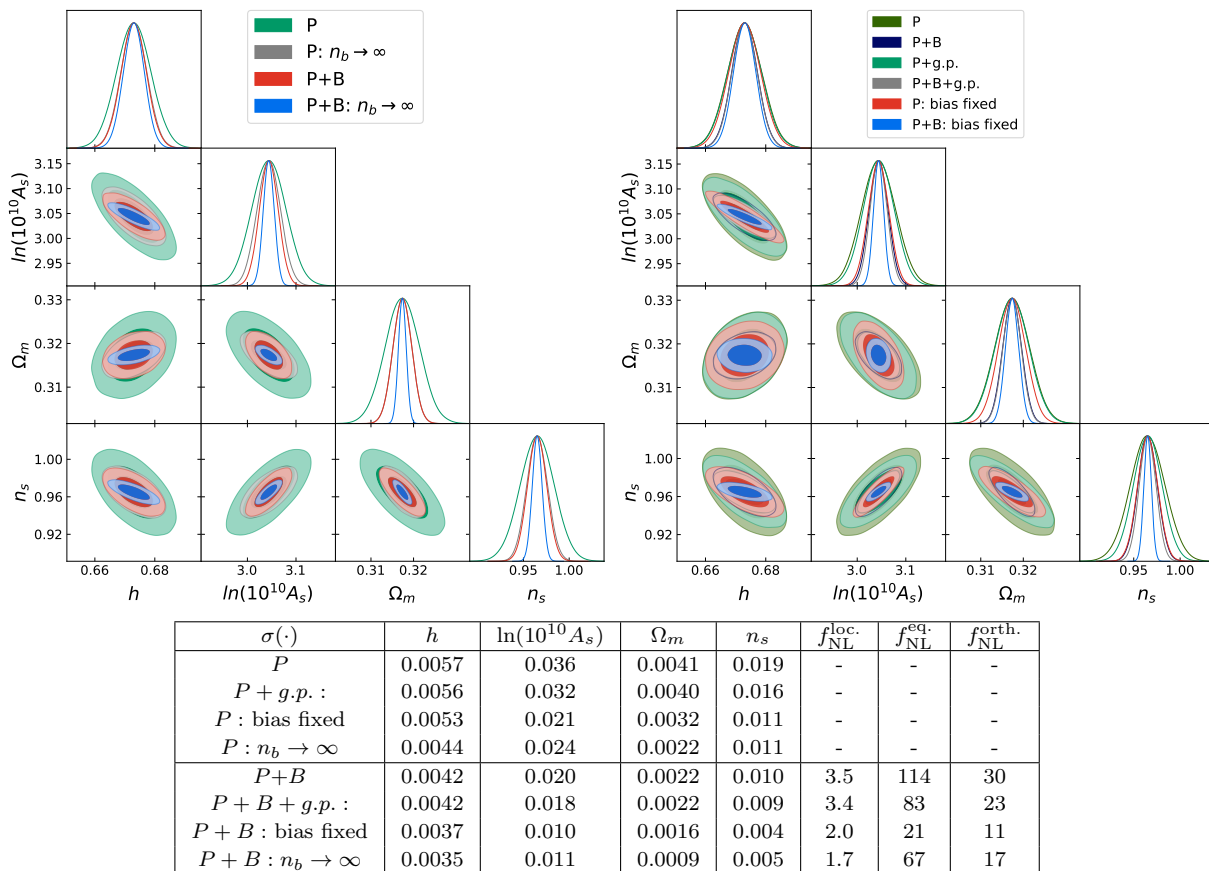


Figure 6: Triangle plots and errors from several different Fisher forecasts for DESI. We compare base results to results obtained without shot noise (left) and with biases fixed or with a “galaxy-formation prior” (g.p.) (right). In the table, we also show the impact of including higher multipoles on the power spectrum and bispectrum and also see the impact on f_{NL} . For the constraints on f_{NL} , we fix the other cosmological parameters.

³⁰We note that due to still large shot noise, the 2-loop analysis for DESI does not much improve the results, which we verified with the same method as mentioned in footnote ²⁸.

4.3 MegaMapper

For MegaMapper, we base our Fisher forecasts on the two scenarios mentioned in [89] (there called “idealized” and “fiducial”), which we call the optimistic (MMo) and pessimistic (MMp) scenarios. These two scenarios are in turn based on the specifications presented in Tab. 1 (MMo) and Tab. 2 (MMp) of [117]. It is important to note that these specifications are preliminary and may differ from the final specifications. We caution that our results are based on these preliminary specifications and may need to be revised as more information becomes available. We find that the constraints predicted by the two scenarios differ by 30 – 40%. Given the similarity of the results in these two situations, we present here the results in the optimistic scenario, leaving the pessimistic scenario in App. B.1. Thus, the numerical values that we will use in this section were derived from Tab. 1 of [117] and methods from Sec. 2. They are given in Tab. 3.

| MMo: | z_{eff} | $n_{b,\text{eff}}[(h \text{ Mpc}^{-1})^3]$ | b_1^{ref} | $(k_{\text{max}}^{\text{Tree}}, k_{\text{max}}^{1L}, k_{\text{NL}}) [h \text{ Mpc}^{-1}]$ | N_{bins}^{1L} | N_{Δ}^{Tree} | N_{Δ}^{1L} |
|-------|------------------|--|--------------------|---|------------------------|----------------------------|-------------------|
| Bin 1 | 2.4 | 1.8×10^{-3} | 3.1 | (0.14, 0.36, 3.2) | 73 | 62 | 696 |
| Bin 2 | 4.3 | 1.1×10^{-4} | 6.3 | (0.28, 0.76, 10.1) | 153 | 294 | 5491 |

Table 3: MegaMapper effective survey specifications, calculated according to the formulas in Sec. 2 and Tab. 7 in App. A. $n_{b,\text{eff}}$ is the background galaxy number density entering the derivatives (not the covariance), N_{bins} is the number of k -bins we consider for the power spectrum at 1-loop and N_{Δ} is the number of triangles we consider for the bispectrum at 1-loop.

As in the DESI forecast, we shift the rest of the biases parameters according to the method described in Sec. 2.3. Furthermore, we again use $k_{\text{min}} = 0.001h \text{ Mpc}^{-1}$ for the power spectrum and $k_{\text{min}} = 0.02h \text{ Mpc}^{-1}$ for the bispectrum, as well as $\Delta k = 0.005h \text{ Mpc}^{-1}$ for the power spectrum and $\Delta k = 0.02h \text{ Mpc}^{-1}$ for the bispectrum. Again, to reduce binning effects, we evaluate on k_{eff} . The results for f_{NL} were again obtained with fixed cosmological parameters. Analyzing f_{NL} in combination with cosmological parameters changes the f_{NL} constraints by less than 3%. Finally, just like for the DESI forecasts, we use the analytical covariance from Eq. (2.16) and Eq. (2.17), following the discussion in Sec. 2.3 and its precision discussed in Sec. 3.

Results We present base results for MegaMapper in a similar format to the previous sections in Fig. 7. We see that the bispectrum contains significant constraining power. As mentioned in Sec. 3.2, we expect that the constraints presented here will be an overestimate as we are neglecting cross-correlations. Nevertheless, the impact of the bispectrum at higher k_{max} becomes relatively more important, and therefore continues to be a very important tool for future data analyses.

In particular, shown in in Fig. 7, the inclusion of the bispectrum allows for very tight constraints on neutrino masses. Even with the caveats discussed in footnote ¹⁷, neutrino mass detection with MegaMapper seems very likely.

Impact of shot noise and biases Given the long timeline until results will be available for MegaMapper, and target selection is yet to happen, we will discuss some aspects that might improve results as was discussed for DESI in Sec. 4.2. In particular, while the perturbative reach

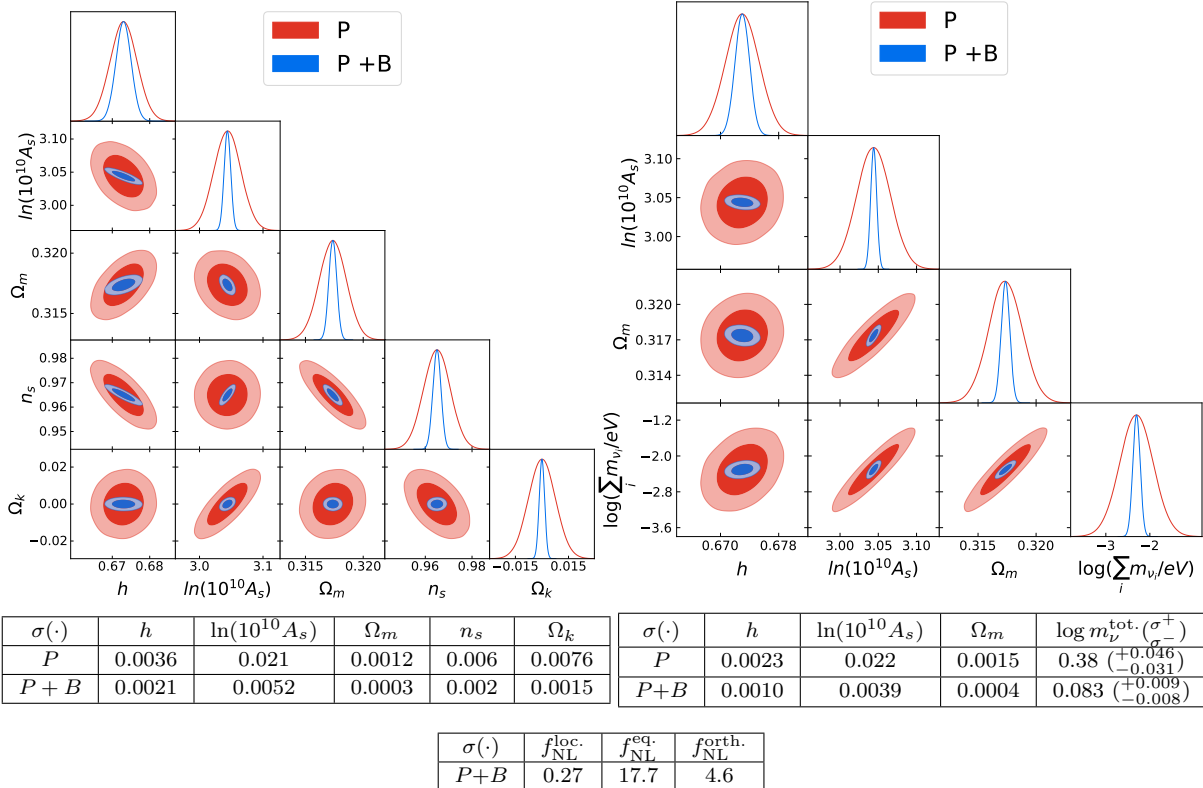


Figure 7: Triangle plots and errors from Fisher forecasts for MegaMapper including the spectral tilt and spatial curvature (left) and massive neutrinos (right) and non-Gaussianity (bottom). In the table we also report the upper and lower bounds of the 68% confidence interval for the sum of massive neutrinos, i.e $\mathbb{P}[(\sum_i m_{\nu_i} - \sum_i m_{\nu_i}^{\text{ref}}) \in (\sigma^-, \sigma^+)] = 0.68$. We use all power spectrum and bispectrum multipoles for the above results and use the analytical covariance without cross-correlations.

is far greater at higher redshifts, as can be seen from Tab. 8, the shot noise, especially for the higher redshift bin, is extremely large³¹. We, therefore, present the limiting case of zero shot noise to better understand the possible gain achievable by reducing the currently estimated shot noise. Equally motivated by the long timeline of MegaMapper, we present results with stronger bias priors, anticipating the better understanding of galaxy formation until the data release. Along with the zero shot noise and “galaxy-formation prior” results, we also present the impact of fixing biases in Fig. 8.

We see that stronger bias priors mostly have an effect on $f_{\text{NL}}^{\text{eq.}}$ and $f_{\text{NL}}^{\text{orth.}}$. Going further and fixing the biases we would again, roughly, reduce the error bar by a factor 2, with again the exception of $f_{\text{NL}}^{\text{eq.}}$ where the dependence is much stronger. This again motivates the perturbativity prior we discuss in Sec. 5. This is very similar to the case of BOSS and DESI shown in Secs. 4.1 and 4.2. Thus, the relative gain of putting the “galaxy-formation prior” or fixing the biases is very similar among the three surveys we consider.

³¹This also means that the 2-loop analysis for MegaMapper just marginally improves on this results at $< 20\%$ error bar reduction, which we verified with the same method as mentioned in footnote²⁸.

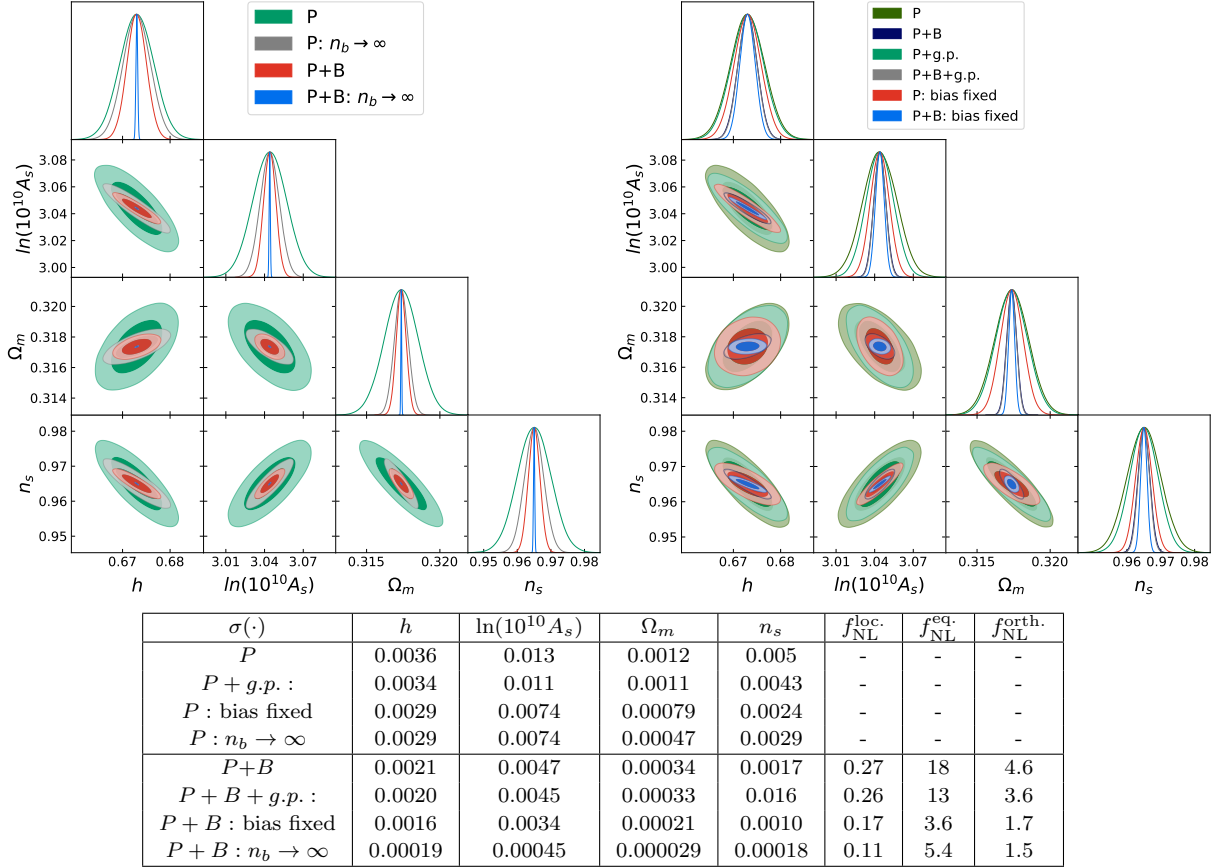


Figure 8: Triangle plots and errors from several different Fisher forecasts for MegaMapper. We compare base results to results obtained without shot noise (left) and with biases fixed or with a “galaxy-formation prior” (g.p.) (right). In the table, we also show the impact of including higher multipoles on the power spectrum and bispectrum and also see the impact on f_{NL} . For the constraints on f_{NL} , we fix the other cosmological parameters.

However, shot noise affects the three surveys very differently. In particular, for MegaMapper, shot noise is quite significant for some cosmological parameters. Especially for the base parameters, we can see from the table in Fig. 8, that reduction of shot noise for MegaMapper can lead to a ~ 10 -fold error bar reduction. Instead for non-Gaussianity parameters, while shot noise still seems to be an important factor, it is comparably less significant. In particular, the effect of setting shot noise to zero is similar to fixing the biases when analyzing f_{NL} .

5 Further constraining f_{NL} with a perturbativity prior

As we have seen in Sec. 4, in particular Figs. 4, 6 and 8, fixing the biases leads to stronger constraints on the primordial parameters $\ln(10^{10}A_s)$ and n_s and to vast improvements on some f_{NL} parameters. We will see in this section that some non-Gaussianity parameters are greatly affected by EFT parameter constraints. In particular, small improvements on the constraints on the bias parameters can lead to significant improvements on $f_{\text{NL}}^{\text{eq.}}$ and $f_{\text{NL}}^{\text{orth.}}$. We are thus motivated

to place stronger (and physically justifiable) priors on the nuisance parameters in order to further constrain single-field inflation.

As mentioned in Sec. 2.3, we put independent priors on the EFT parameters, restricting their individual size. This is motivated by the fact that the EFTofLSS predicts these parameters to be of order one. However, given that the MCMC explores the full parameter space in a random walk, the final loop contribution can be \sqrt{n} larger than the truth, where n is the number of EFT parameters. We aim to address the issue that such parameter configurations are unphysical yet can still fit the data well. This happens because, at intermediate and low k 's, where each term is not too small, even a too-large loop is comparably small with respect to the data error that scales like $k^{-3/2}$. Therefore, only at large k where the data error is sufficiently small, would parameter configurations exhibiting \sqrt{n} enhancements to the loop be ruled out. However, there exist parameter configurations exhibiting \sqrt{n} larger contributions at lower k 's that cancel out at large k , making the loop appear to have the correct size at those scales. Therefore, a loop contribution that is too large at low k can still fit the data well, but would go unnoticed, even though it would clearly be unphysical. Through scaling relations, this then translates to an overestimate of the expected higher loop contribution. This argument is shown for the estimated 2-loop contribution in Fig. 9.

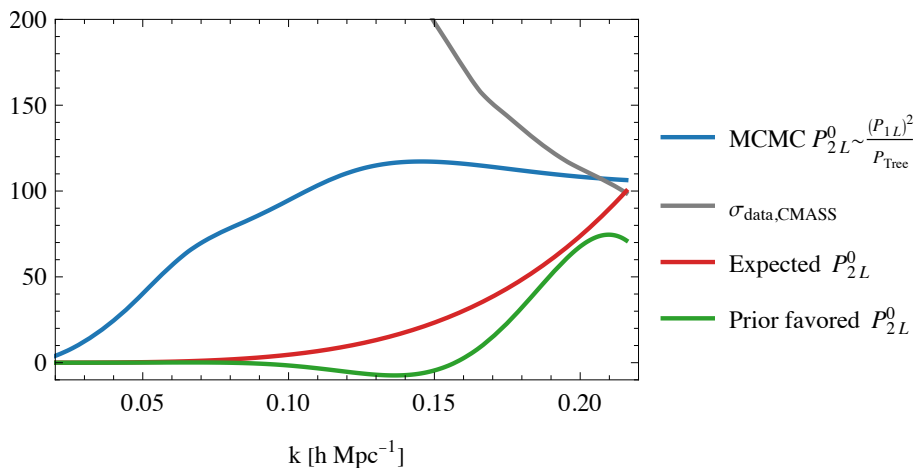


Figure 9: Plot showing various two-loop monopole power spectra, P_{2L}^0 against the CMASS data error, $\sigma_{\text{data,CMASS}}$ (grey). As an example of a typical MCMC, the BOSS CMASS P_{2L}^0 was estimated using the relation $P_{2L} \sim \frac{P_{1L}^2}{P_{\text{Tree}}}$, and is shown in blue. The expected P_{2L}^0 size is shown in red and an example of a P_{2L}^0 that would be favoured by the perturbativity prior is shown in green.

We, therefore, propose an additional prior, which we call “perturbativity prior”, on the size of the loop contributions, aimed at being effective in the intermediate and low k regions where the \sqrt{n} enhancements are not sufficiently restricted by the data analysis. To formulate this “perturbativity prior”, we use the fact that, as we sample the different bias configurations, the two-loop contribution can have a maximal size, and therefore a maximal signal-to-noise. This maximal signal-to-noise was what defined the k_{max} in Eq. (2.22). In this section, we show that by using

appropriate scaling relations between the two-loop and one-loop contributions, we can translate this threshold for the two-loop contribution into a prior on the size of the one-loop contribution.

5.1 Contribution to the Fisher matrix

We impose a perturbativity prior for the power spectrum and bispectrum respectively, and the procedure is the same in both cases. We therefore keep the derivation generic, for the loop of some observable, X_{1L} , where $X \in \{P, B\}$. In a later step, we will derive an estimate for the correct size of the loop, denoted by X_{1L}^C . As mentioned in the previous section, this estimate will come from a threshold for the signal-to-noise of two-loop contributions, through which we can infer properties about the correct one-loop contributions. The quantity we want to constrain is X_{1L} , whereas X_{1L}^C we assume to be estimated before the data analysis. We then impose that on average, X_{1L} is close to X_{1L}^C , therefore, we impose a Gaussian prior

$$\frac{1}{N_X} \sum_{k_i} \int_{-1}^1 \int_0^{2\pi} \frac{d\mu_i}{2} \frac{d\phi}{2\pi} \frac{X_{1L}(k_i; \hat{z})}{X_{1L}^C(k_i; \hat{z})} \sim \mathcal{N}(1, 1), \quad (5.1)$$

where $k_i \in \{k, (k_1, k_2, k_3)\}$, $\mu_i \in \{\mu, \mu_1\}$ and $N_X \in \{N_{\text{bins}}, N_{\Delta}\}$ for the power spectrum and bispectrum respectively. We here implement the real space part of the perturbativity prior ³². For the remainder of this section, we, therefore, always refer to real space quantities, indicated by dropping the \hat{z} argument. The real space prior we then impose is given by

$$\frac{1}{N_X} \sum_{k_i} \frac{X_{1L}(k_i)}{X_{1L}^C(k_i)} \sim \mathcal{N}(1, 1). \quad (5.2)$$

One way to write the prior above is to impose the same, independent, prior for each bin. That is, we impose

$$X_{1L}(k_i) \sim \mathcal{N}\left(X_{1L}^C(k_i), N_X \left(X_{1L}^C(k_i)\right)^2\right), \quad (5.3)$$

which implies Eq. (5.2).

In order to use this prior for the Fisher matrix, we assume once again that our reference cosmology is accurate and we assume $X_{1L}^{\text{ref}} \simeq X_{1L}^C$ (³³). Then, for fixed k_i , similarly to Eq. (2.3),

³²We note that the real space perturbativity prior is on its own only restricting the size of the real space correlators. However, given that the size of the full redshift space observables is highly dependent on the real space EFT-parameter values, there is little room left for the full redshift space contribution to be large, if the real space contribution is restricted enough. We therefore expect that the full redshift space prior is highly correlated with the real space one, and, therefore, only do the real space version here. Adding the redshift space part is straightforward.

³³Given that the best-fit we currently have was not obtained with the use of the perturbativity prior, this approximation is not guaranteed to be justified. However, as we will see in Fig. 10, the perturbativity prior only mildly affects the errors of EFT parameters. Therefore, we assume that the best-fit values are also only slightly modified, still making the reference values we use here, a good approximation. This issue will disappear once a data analysis with this additional prior is performed.

we can Taylor expand to get ³⁴

$$\begin{aligned} -2 \log \text{Prior} &= \frac{1}{N_X (X_{1L}^C)^2} (X_{1L}(\theta) - X_{1L}^C)^2 + r_1 \\ &\simeq (\theta - \theta^{\text{ref}})^T F^{X,\text{pert.}} (\theta - \theta^{\text{ref}}) + r_1, \end{aligned} \quad (5.4)$$

where $F_{ij}^{X,\text{pert.}} = \frac{1}{N_X (X_{1L}^C)^2} \frac{\partial X_{1L}}{\partial \theta_i} \frac{\partial X_{1L}}{\partial \theta_j}$ and r_1 is a parameter-independent constant. Therefore, summing over all bins, the perturbativity prior that we finally implement in the Fisher forecast is given by

$$\begin{aligned} F_{ij}^{\text{pert.}} &= \frac{1}{N_{\text{bins}}} \sum_k \frac{1}{P_{1L}^C(k)^2} \frac{\partial P_{1L}(k)}{\partial \theta_i} \frac{\partial P_{1L}(k)}{\partial \theta_j} \\ &\quad + \frac{1}{N_{\Delta}} \sum_{k_1, k_2, k_3} \frac{1}{B_{1L}^C(k_1, k_2, k_3)^2} \frac{\partial B_{1L}(k_1, k_2, k_3)}{\partial \theta_i} \frac{\partial B_{1L}(k_1, k_2, k_3)}{\partial \theta_j}. \end{aligned} \quad (5.5)$$

In order to be able to implement this prior, we need to derive the estimates for P_{1L}^C and B_{1L}^C . We derive the threshold for the size of the 1-loop contributions from limiting the 2-loop signal-to-noise ratio. This is similar to how we determined the k_{max} in Sec. 2.3. There, we demanded that the signal-to-noise of the 2-loop contribution for any new survey does not exceed its signal-to-noise of BOSS CMASS, where we know it is negligible. In particular, the maximal signal-to-noise that has previously been chosen in the data analysis to determine the k_{max} was $\frac{1}{9}$, which is also what we use here. Explicitly,

$$\begin{aligned} \int_0^{k_{\text{max}}} \left(\frac{P_{2L}(k)}{\tilde{\sigma}_{P,\text{data}}(k)} \right)^2 dk &\simeq \frac{1}{9}, \\ \int_{\nu_B} \left(\frac{B_{2L}(k_1, k_2, k_3)}{\tilde{\sigma}_{B,\text{data}}(k_1, k_2, k_3)} \right)^2 dk_1 dk_2 dk_3 &\simeq \frac{1}{9}, \end{aligned} \quad (5.6)$$

where $\tilde{\sigma}_{X,\text{data}}$ here is defined as in Eq. (2.25), using that in the continuum limit we get $\Delta k \rightarrow dk$, and ν_B is the set of all triangles with maximal wavenumber smaller than or equal to k_{max} . We then get the estimates for the correct one-loop contributions, through the approximate size relations between two-loop and one-loop, $P_{2L} \sim \frac{P_{1L}^C{}^2}{P_{\text{Tree}}^{NS}}$ and $B_{2L} \sim \frac{B_{1L}^C P_{1L}^C}{P_{\text{Tree}}^{NS}}$ (35). Finally, in order to perform the integrals in Eq. (5.6), we assume scaling functions $S^X(k_i)$, defined by $\frac{S^X(k_i)}{S^X(k_{\text{max}})} = \frac{X_{1L}^C(k_i)}{X_{1L}^C(k_{\text{max}})}$ (36), that should approximate the k dependencies of $X_{1L}^C(k_i)$. Plugging in the size relations and scaling

³⁴ We would not need to do this Taylor expansion in an actual data analysis.

³⁵ Note that here the numerators have the usual stochastic contributions, but P_{Tree}^{NS} in the denominators has no shot noise.

³⁶ One could have normalized this scaling factor to make it unitless, *i.e.* $S^X(k_i) \rightarrow \frac{S^X(k_i)}{S^X(k_{\text{max}})}$ without changing anything in the final formulas.

approximation into Eq. (5.6), we can solve for the $X_{1L}^C(k_i)$ to get

$$P_{1L}^C(k) = S^P(k) \left(9 \int_0^{k_{\max}} \left(\frac{S^P(k')^2}{P_{\text{Tree}}^{NS}(k') \tilde{\sigma}_{P,\text{data}}(k')} \right)^2 dk' \right)^{-1/4}, \quad (5.7)$$

$$B_{1L}^C = S^B(k_1, k_2, k_3) \left(9 \int_{\nu_B} \left(\frac{S^B(k'_1, k'_2, k'_3)}{\tilde{\sigma}_{B,\text{data}}(k'_1, k'_2, k'_3)} \frac{1}{3} \left(\frac{P_{1L}^C(k'_1)}{P_{\text{Tree}}^{NS}(k'_1)} + 2p \right) \right)^2 dk'_1 dk'_2 dk'_3 \right)^{-1/2},$$

where we dropped the k -dependence for B_{1L}^C to avoid clutter and in the bottom line we symmetrize the $\frac{P_{1L}^C}{P_{\text{Tree}}^{NS}}$. Note that P_{1L}^C and B_{1L}^C do not depend on the overall size of the scaling estimates S^X , as we are normalizing it at k_{\max} .

There are well established estimates for the behaviour of the power spectrum loop [40] and bispectrum loop [122] in a scaling universe. For biased tracers we adapt this to

$$S_{\text{int}}^P(k) = P_{\text{Tree}}(k) \left(\frac{k}{k_{\text{NL}}} \right)^{3+n(k)}, \quad (5.8)$$

$$S_{\text{int}}^B(k_1, k_2, k_3) = B_{\text{Tree}}(k_1, k_2, k_3) \left(\left(\frac{k_1}{k_{\text{NL}}} \right)^{3+n(k_1)} + 2p \right),$$

which is very similar to the one used in Eq. (2.23), but with P_{Tree} and B_{Tree} being the (real space) biased tracers tree-level power spectrum and bispectrum. In order to have both the right IR and UV behaviour of the loop contributions we also include a loop counter term to the estimate. For the scaling of the counterterms, we use

$$S_c^P(k) = -2b_1\beta P_{11}(k) \left(\frac{k}{k_{\text{NL}}} \right)^2, \quad (5.9)$$

$$S_c^B(k_1, k_2, k_3) = -2b_1^2\beta \left(P_{11}(k_1)P_{11}(k_2) \left(\frac{k_3}{k_{\text{NL}}} \right)^2 + 2p \right),$$

where we use the reference value $\beta_{\text{BOSS}} = 1$ and rescale with Eq. (2.19) for other surveys³⁷. Finally, given that S^P and S^B should be upper bounds on the the scaling of the loops, we want to avoid cancelations and ensure positivity. Therefore, the final scalings we implement are

$$S^P(k) = \max(|S_{\text{int}}^P(k)|, |S_c^P(k)|), \quad (5.10)$$

$$S^B(k_1, k_2, k_3) = \max(|S_{\text{int}}^B(k_1, k_2, k_3)|, |S_c^B(k_1, k_2, k_3)|).$$

5.2 Results

While the perturbativity prior further constrains both cosmological parameters and bias parameters, the largest effect comes from further constraining particular bias parameters. We present this improvement in Fig. 10. Indeed, there we can see that small improvements on particular EFT

³⁷The representative counter terms here correspond to the terms multiplied by c_1^h and c_3^h in [111].

parameters³⁸ lead to vast improvements on $f_{\text{NL}}^{\text{eq.}}$. In the tables of Fig. 10 we also show the effect on the other types of non-Gaussianity we analyze. Each analysis was performed with fixed cosmological parameters and each type of non-Gaussianity was analyzed separately. For completeness, and to stress the importance of the bispectrum loop, we also compare it with bispectrum tree-level constraints. The survey specifications used for the tree-level analysis are also in Tabs. 1, 2, and 3. In the following, we will present results for each survey based on the plots in Fig. 10.

Finally, as we also discussed in Sec. 4, base cosmological parameters are less affected by constraints on bias parameters. However, we find that the inclusion of the perturbativity prior can have a relevant effect on them, which we discuss in App. B.2. In particular, we find that DESI will constrain curvature to 0.012 and MegaMapper to 0.0012.

BOSS As shown in the table of Fig. 10, the one-loop bispectrum already significantly improves the constraints on non-Gaussianities by $\sim 30 - 50\%$ with respect to the tree-level analysis. Additionally including the perturbativity prior to the one-loop bispectrum yields a further $\sim 24\%$ reduction in σ for $f_{\text{NL}}^{\text{loc.}}$, and $\sim 10\%$ reduction in σ for $f_{\text{NL}}^{\text{eq.}}$ and $f_{\text{NL}}^{\text{orth.}}$. The “galaxy-formation prior” would further reduce the error by $\sim 20 - 30\%$ for $f_{\text{NL}}^{\text{eq.}}$ and $f_{\text{NL}}^{\text{orth.}}$, and 14% for $f_{\text{NL}}^{\text{loc.}}$. The addition of the loop breaks the degeneracy between c_2 and c_4 (39), greatly improving constraints on both parameters, which translates to stronger constraints on $f_{\text{NL}}^{\text{eq.}}$. Furthermore, the inclusion of the perturbativity prior further breaks this degeneracy and improves upon the constraints on b_1 , which leads to additional improvements on the f_{NL} parameters.

DESI As it was seen in BOSS, the inclusion of the loop bispectrum and perturbativity prior breaks the degeneracy between c_2 and c_4 and tightens the constraints on EFT parameters for DESI as well. However, the resulting effect on f_{NL} parameters is different. Unlike BOSS, the inclusion of the one-loop bispectrum and perturbativity prior to DESI does not uniformly tighten all f_{NL} errors. For one, most of the information to constrain $f_{\text{NL}}^{\text{loc.}}$ is contained in the power spectrum and the tree-level bispectrum. In contrast, the one-loop bispectrum does improve the constraint of $f_{\text{NL}}^{\text{eq.}}$ and $f_{\text{NL}}^{\text{orth.}}$ by 19% and 58% respectively. The perturbativity prior reduces these errors further by 20% and 11% and the future galaxy formation prior by another 16% and 19%.

MegaMapper MegaMapper results are more similar to DESI than BOSS. $f_{\text{NL}}^{\text{loc.}}$ is mostly constrained through the power spectrum and does not improve much with the addition of the bispectrum loop or the perturbativity prior. Additionally, as was seen for DESI, the inclusion of the bispectrum loop leads to a more significant improvement in the constraint on $f_{\text{NL}}^{\text{orth.}}$ compared to $f_{\text{NL}}^{\text{eq.}}$, with 47% and 24% improvements respectively. To place these results into context, note that the tree level results we obtain are in agreement with those obtained in [102]⁴⁰. Note, however,

³⁸We remind the reader that c_2 and c_4 are the second-order biases that enter the tree-level bispectrum, alongside the linear bias b_1 . For more details see [110, 111].

³⁹The breaking of this degeneracy due to the loop bispectrum is already present in [110].

⁴⁰The results we present here would correspond to their MegaMapper - B results, with fixed cosmological parameters and free bias parameters. The disagreement with our results is $< 10\%$.

the tree-level k_{max} we estimate here is a bit lower, thus we predict slightly less optimistic constraints for the tree-level bispectrum, which makes the addition of the loop more important. The loop again breaks the degeneracy between c_2 and c_4 , and the perturbativity prior enhances the constraints on c_2 in particular, thereby improving the constraints on $f_{\text{NL}}^{\text{eq}}$ and $f_{\text{NL}}^{\text{orth}}$ by 9% and the “galaxy-formation prior” further reduces the errors by 21% and 18% respectively.

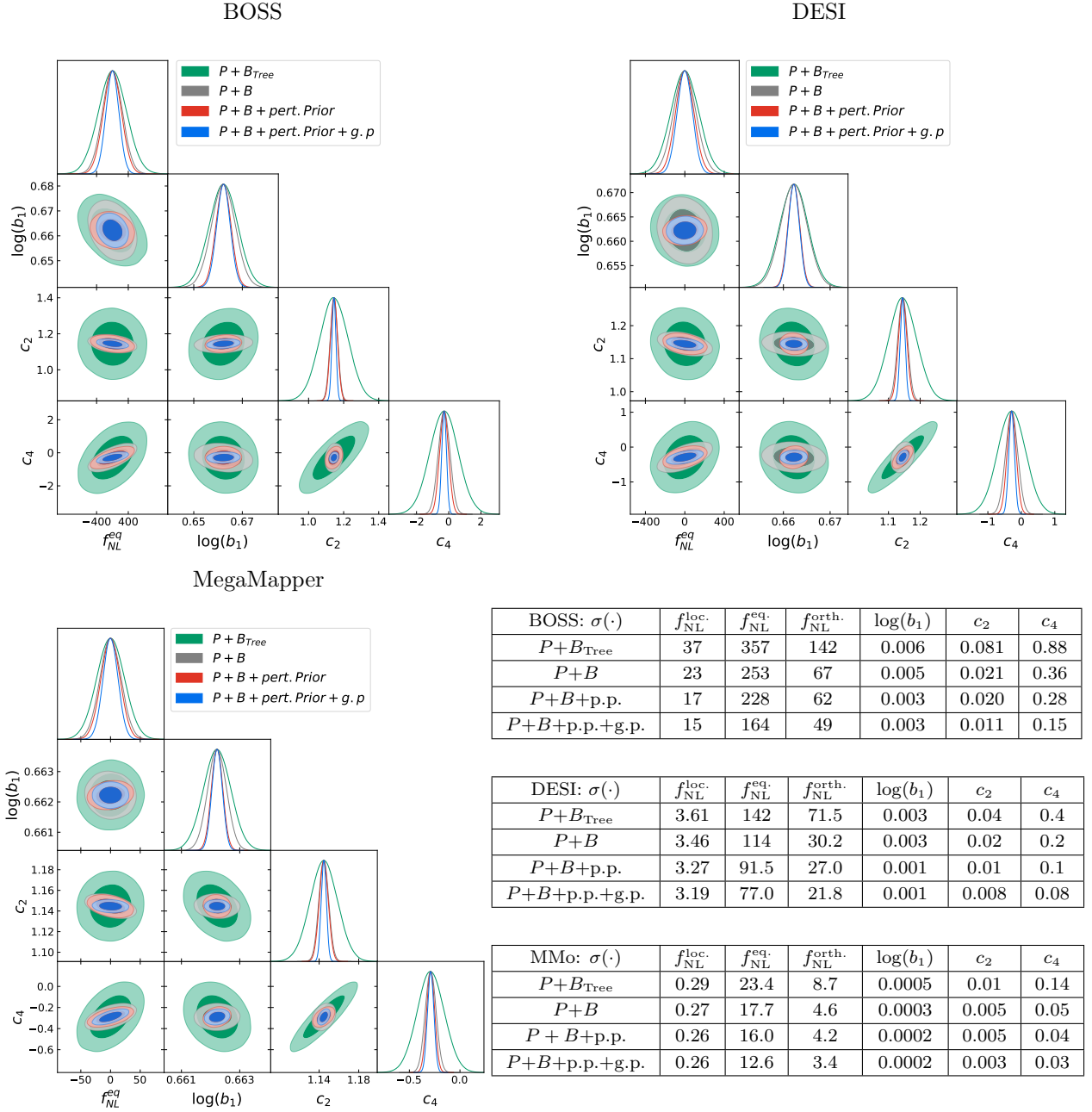


Figure 10: Triangle plots and errors from Fisher forecasts for BOSS (top left), DESI (top right), and MegaMapper (bottom left), for the equilateral type of non-Gaussianity, and leading bias parameters. We also show errors on other non-Gaussianity parameters in the tables. Each analysis was done with cosmological parameters fixed and each non-Gaussianity parameter was analyzed separately. We always include the power spectrum at one loop order with the addition of either the tree-level bispectrum the loop bispectrum or the loop bispectrum with a perturbativity prior (p.p.) also in combination with the “galaxy-formation prior” (g.p.). We use all power spectrum and bispectrum multipoles in each case and use the analytical covariance without cross-correlations.

Acknowledgements

We are very grateful for conversations with Guido D’Amico, Eva Silverstein and Pierre Zhang and for providing their results from the BOSS MCMC. Y.D. would like to thank Enrico Pajer, Blake Sherwin, Paul Shellard, James Fergusson, and Daniel Glazer for useful discussions. Y.D. acknowledges support from the STFC. LS is supported by the SNSF grant 200021_213120.

A Survey details and best-fits

Shown below are the exact parameter values that we use in the analyzes for each survey. Regarding cosmological parameters, for all surveys, we use the following best-fit as the reference cosmology ⁴¹ for the cosmological parameters (noted with a ^{ref}).

$$\begin{aligned}
 h^{\text{ref}} = 0.673, \quad \ln(10^{10} A_s)^{\text{ref}} = 3.044, \quad \Omega_m^{\text{ref}} = 0.317, \quad n_s^{\text{ref}} = 0.965, \quad (\text{A.1}) \\
 \Omega_k^{\text{ref}} = 0, \quad \omega_b^{\text{ref}} = 0.022, \quad \sum_i m_{\nu_i}^{\text{ref}} = 0.1 \text{ eV}, \quad f_{\text{NL}}^{\text{loc.,ref}} = f_{\text{NL}}^{\text{eq.,ref}} = f_{\text{NL}}^{\text{orth.,ref}} = 0.
 \end{aligned}$$

Furthermore, in Tab. 4 we give the EFT parameter best-fit that we use, coming from [110]. Note, this is what we denote as \vec{b}_{BOSS} (b1 - Bc14) and \vec{c}_{BOSS} (Bd1 - Be12) in Sec. 2.3. Furthermore, we use the notation as in PyBird [18]. For a conversion to the notation of [110], see App. D.4 of [110]. The best-fit values of the 41 EFT parameters are given in Tab. 4.

| Parameter | Value | Parameter | Value | Parameter | Value | Parameter | Value |
|-----------|-------|-----------|--------|-----------|--------|-----------|-------|
| b1 | 1.94 | c2 | 1.14 | b3 | -0.37 | c4 | -0.29 |
| b4 | 0.13 | b6 | -0.35 | b7 | 0.22 | b8 | -0.30 |
| b9 | 0.015 | b10 | 0.043 | b11 | 0.036 | Bc1 | 5.46 |
| Bc2 | -1.54 | Bc3 | 1.31 | Bc4 | -0.48 | Bc5 | 0.11 |
| Bc6 | 0.87 | Bc7 | -0.46 | Bc8 | 0.44 | Bc9 | -0.42 |
| Bc10 | -0.65 | Bc11 | -0.088 | Bc12 | -0.37 | Bc13 | -0.16 |
| Bc14 | -0.20 | Bd1 | 5.4 | Bd2 | -0.72 | Bd3 | -0.43 |
| ce2 | 0.55 | Be1 | 1.69 | Be2 | 0.91 | Be3 | 0.074 |
| Be4 | -0.14 | Be5 | 6.07 | Be6 | -0.093 | Be7 | -0.97 |
| Be8 | 0.26 | Be9 | 0.26 | Be10 | -0.15 | Be11 | 0.43 |
| Be12 | -0.43 | | | | | | |

Table 4: Best-fit EFT parameters.

Next, we show the survey specifications that were used in each survey. With the methods from Sec. 2, this builds the basis for the numerical values that we use in the forecasts.

BOSS For the BOSS survey, we use the survey specifications as presented in [87, 123–125]. We display them in the same way they enter our formulas in Tab. 5.

⁴¹All cosmological parameters with the exception of f_{NL} and $\sum_i m_{\nu_i}$ are fixed to Planck preferred values [6].

| z | N_g | $V[(h^{-1}\text{Mpc})^3]$ | $n_b[(h\text{Mpc}^{-1})^3]$ | b_1 |
|------|--------|---------------------------|-----------------------------|-------|
| 0.05 | 7370 | 2.55×10^7 | 2.9×10^{-4} | 1.48 |
| 0.15 | 47560 | 1.64×10^8 | 2.9×10^{-4} | 1.56 |
| 0.25 | 120600 | 4.02×10^8 | 3.0×10^{-4} | 1.65 |
| 0.35 | 214016 | 7.04×10^8 | 3.0×10^{-4} | 1.73 |
| 0.45 | 287040 | 1.04×10^9 | 2.8×10^{-4} | 1.83 |
| 0.55 | 445740 | 1.38×10^9 | 3.2×10^{-4} | 1.92 |
| 0.65 | 206400 | 1.72×10^9 | 1.2×10^{-4} | 2.02 |
| 0.75 | 20400 | 2.04×10^9 | 1.0×10^{-5} | 2.12 |

Table 5: Survey details for each redshift bin for BOSS. We show the number of mapped galaxies N_g , the volume of the redshift bin V as well as the number density n_b and the linear bias b_1 .

DESI As mentioned in the main text, for DESI we focus on the largest sample which is the set of Emission Line Galaxies. The numerical values we use are calculated from table 2.3 in [88]. We present the specifications in Tab. 6.

| z | N_g | $V[(h^{-1}\text{Mpc})^3]$ | $n_b[(h\text{Mpc}^{-1})^3]$ | b_1 |
|------|--------------------|---------------------------|-----------------------------|-------|
| 0.65 | 432600 | 2.63×10^9 | 1.64×10^{-4} | 1.18 |
| 0.75 | 3.18×10^6 | 3.15×10^9 | 1.01×10^{-3} | 1.23 |
| 0.85 | 2.70×10^6 | 3.65×10^9 | 7.38×10^{-4} | 1.29 |
| 0.95 | 2.93×10^6 | 4.1×10^9 | 7.15×10^{-4} | 1.35 |
| 1.05 | 2.02×10^6 | 4.52×10^9 | 4.46×10^{-4} | 1.41 |
| 1.15 | 1.89×10^6 | 4.89×10^9 | 3.87×10^{-4} | 1.47 |
| 1.25 | 1.87×10^6 | 5.22×10^9 | 3.59×10^{-4} | 1.53 |
| 1.35 | 732200 | 5.5×10^9 | 1.33×10^{-4} | 1.59 |
| 1.45 | 652400 | 5.75×10^9 | 1.13×10^{-4} | 1.65 |
| 1.55 | 460600 | 5.97×10^9 | 7.71×10^{-5} | 1.72 |
| 1.65 | 176400 | 6.15×10^9 | 2.87×10^{-5} | 1.78 |

Table 6: Survey details for each redshift bin for DESI. We show the number of mapped galaxies N_g , the volume of the redshift bin V as well as the number density n_b and the linear bias b_1 .

MegaMapper Finally, for MegaMapper, the specifications are still to be finalized given the early stage of the experiment compared to BOSS or DESI. We take the numerical values from [117, 89], where as mentioned in the main text there is an “idealized”, and a “fiducial” scenario. The specifications for the optimistic (or “idealized”) scenario are in Tab. 7. They are based on Tab. 1 of [117]. For the “fiducial” or what we call “pessimistic” scenario, we refer to table 2 in [117].

| z | N_g | $V[(h^{-1}\text{Mpc})^3]$ | $n_b[(h\text{Mpc}^{-1})^3]$ | b_1 |
|-----|--------------------|---------------------------|-----------------------------|-------|
| 2 | 6.75×10^7 | 2.70×10^{10} | 2.5×10^{-3} | 2.5 |
| 2.5 | 3.32×10^7 | 2.76×10^{10} | 1.2×10^{-3} | 3.3 |
| 3 | 1.63×10^7 | 2.72×10^{10} | 6×10^{-4} | 4.1 |
| 3.5 | 7.88×10^6 | 2.63×10^{10} | 3×10^{-4} | 4.9 |
| 4 | 3.76×10^6 | 2.51×10^{10} | 1.5×10^{-4} | 5.8 |
| 4.5 | 1.90×10^6 | 2.38×10^{10} | 8×10^{-5} | 6.6 |
| 5 | 901730 | 2.25×10^{10} | 4×10^{-5} | 7.4 |

Table 7: Survey details for each redshift bin for MegaMapper (optimistic). We show the number of mapped galaxies N_g , the volume of the redshift bin V as well as the number density n_b and the linear bias b_1 .

B Further analyses

Two further analyses, which to us do not carry the same significance as those presented in the main sections, are presented here for completeness. In Sec. B.1 we present results for the ‘‘pessimistic’’ scenario for MegaMapper as opposed to the ‘‘optimistic’’ scenario presented in Sec. 4.3. In Sec. B.2 we also present the impact of the perturbativity prior, as discussed in Sec. 5, on base cosmological parameters.

B.1 MegaMapper ‘‘pessimistic’’ results

The survey specifications for the ‘‘pessimistic’’ scenario given in Tab. 8 are determined with the methods described in Sec. 2.

| MMp: | z_{eff} | $n_{b,\text{eff}}[(h\text{Mpc}^{-1})^3]$ | b_1 | $(k_{\text{max}}^{\text{Tree}}, k_{\text{max}}^{1L}, k_{\text{NL}}) [h\text{Mpc}^{-1}]$ | N_{bins}^{1L} | N_{Δ}^{Tree} | N_{Δ}^{1L} |
|-------|------------------|--|-------|---|------------------------|----------------------------|-------------------|
| Bin 1 | 2.1 | 8.8×10^{-4} | 2.7 | (0.12, 0.31, 2.2) | 62 | 43 | 428 |
| Bin 2 | 4.3 | 8.4×10^{-5} | 4.0 | (0.21, 0.57, 8.2) | 114 | 150 | 2331 |

Table 8: MegaMapper ‘‘pessimistic’’ effective survey specifications, calculated according to the formulas in Sec. 2. $n_{b,\text{eff}}$ is the background galaxy number density entering the derivatives (not the covariance), N_{bins} is the number of k -bins we consider for the power spectrum at 1-loop and N_{Δ} is the number of triangles we consider for the bispectrum at 1-loop.

To avoid redundancy with the discussion of the optimistic scenario, we here simply focus on base results for the pessimistic MegaMapper scenario. The discussion on fixing biases, shot noise and the inclusion of the perturbativity prior is comparable to the optimistic case. The only difference are the absolute values, while the relative gains are similar. We present results in Fig. 11, where we present the same base parameters as in the main section. Comparing to the figure and tables in Fig. 7 for almost all parameters we see only a 30 – 40% difference compared to the optimistic case. The non-Gaussianity scenarios all differ by roughly 40 – 45%, independent on whether we use the tree-level bispectrum, the loop, or the perturbativity prior.

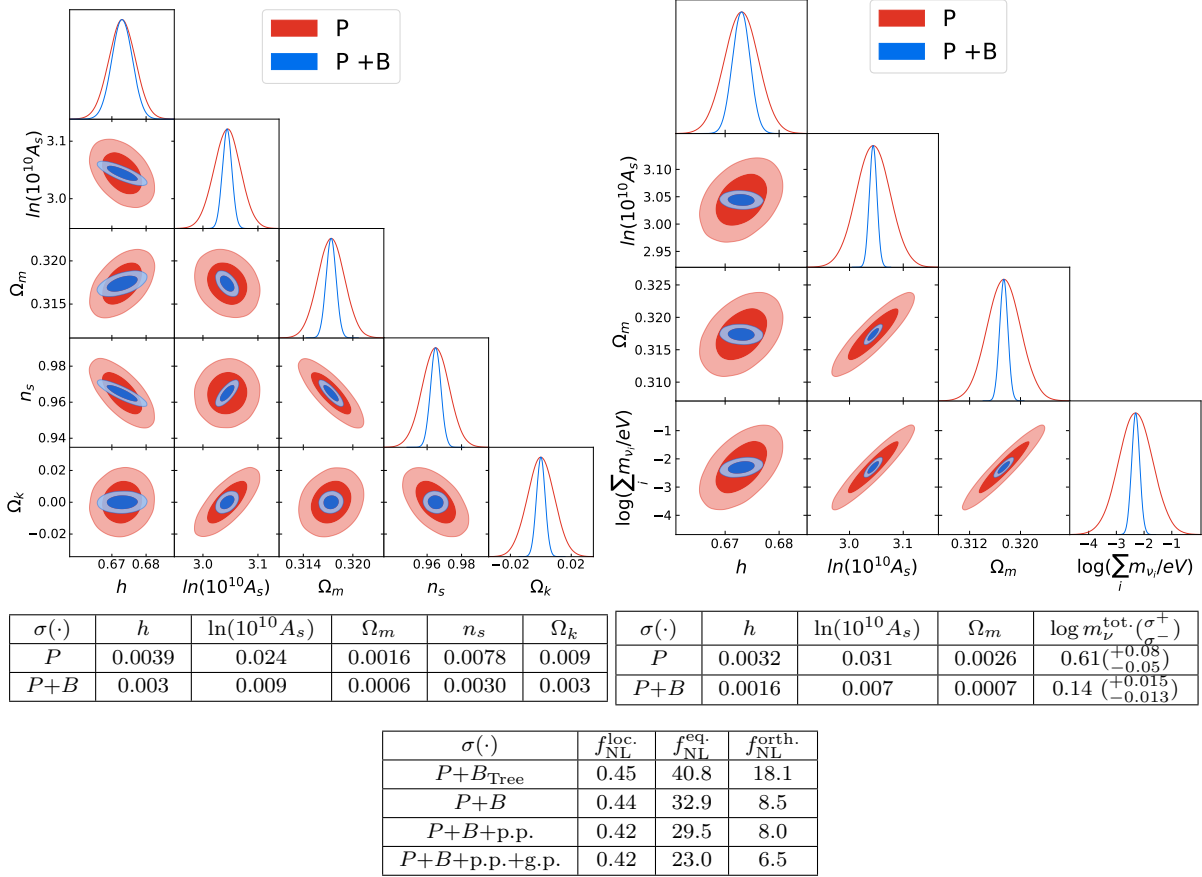


Figure 11: Triangle plots and errors from Fisher forecasts for MegaMapper (pessimistic) including the spectral tilt and spatial curvature (left) and massive neutrinos (right) and Non-Gaussianity (bottom). We use all power spectrum and bispectrum multipoles for the above results, and use the analytical covariance without cross-correlations. In the table we also report the upper and lower bounds of the 68% confidence interval for the sum of massive neutrinos, i.e $\mathbb{P}[(\sum_i m_{\nu_i} - \sum_i m_{\nu_i}^{\text{ref}}) \in (\sigma^-, \sigma^+)] = 0.68$. For non-Gaussianity, we also present results with only the inclusion of the tree-level bispectrum and with the inclusion of a perturbativity prior (p.p) and the “galaxy-formation prior” (g.p.).

B.2 Perturbativity prior effect on base cosmological parameters

We discuss here the effect of the perturbativity prior, also in combination with the galaxy formation prior, on base cosmological parameters. Results for all surveys are shown in Fig. 12. We see that the most notable effect is on $\ln(10^{10} A_s)$, n_s and Ω_k , and a smaller effect on the other parameters. Furthermore, we found almost no improvement on constraints for neutrino masses.

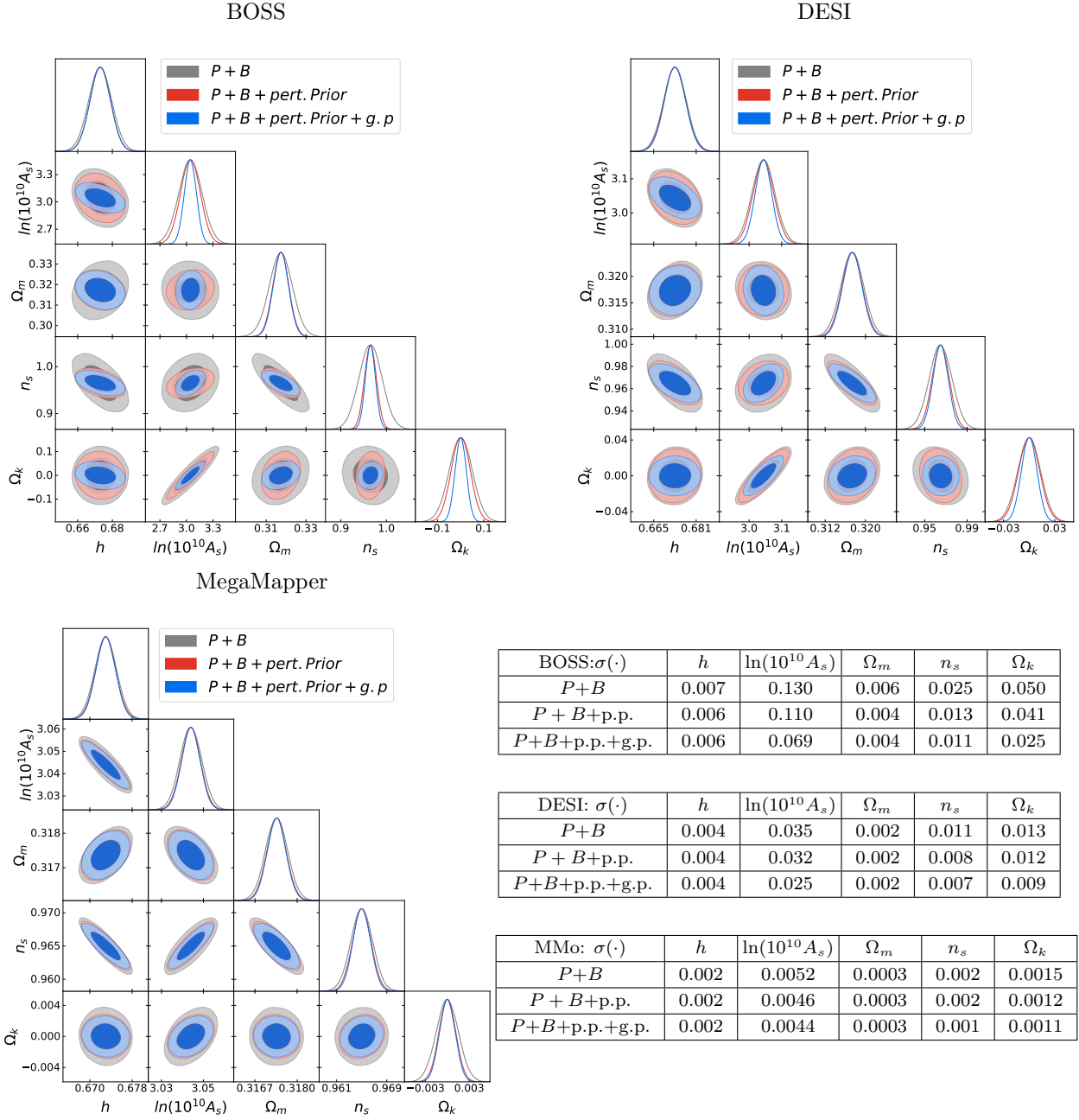


Figure 12: Triangle plots and errors from Fisher forecasts for BOSS (top left), DESI (top right), and MegaMapper (bottom left), for base cosmological parameters including the spectral tilt and spatial curvature. We always include the power spectrum at one loop order with the addition of either the loop bispectrum or the loop bispectrum with a perturbativity prior (p.p.) or also in combination with the “galaxy-formation prior” (g.p.). We use all power spectrum and bispectrum multipoles in each case and use the analytical covariance without cross-correlations.

References

- [1] D. Baumann, A. Nicolis, L. Senatore and M. Zaldarriaga, Cosmological Non-Linearities as an Effective Fluid, [JCAP **1207** \(2012\) 051](#), [[1004.2488](#)].
- [2] J. J. M. Carrasco, M. P. Hertzberg and L. Senatore, The Effective Field Theory of Cosmological Large Scale Structures, [JHEP **09** \(2012\) 082](#), [[1206.2926](#)].
- [3] G. D’Amico, J. Gleyzes, N. Kokron, D. Markovic, L. Senatore, P. Zhang et al., The Cosmological Analysis of the SDSS/BOSS data from the Effective Field Theory of Large-Scale Structure, [JCAP **05** \(2020\) 005](#), [[1909.05271](#)].
- [4] M. M. Ivanov, M. Simonović and M. Zaldarriaga, Cosmological Parameters from the BOSS Galaxy Power Spectrum, [JCAP **05** \(2020\) 042](#), [[1909.05277](#)].
- [5] T. Colas, G. D’Amico, L. Senatore, P. Zhang and F. Beutler, Efficient Cosmological Analysis of the SDSS/BOSS data from the Effective Field Theory of Large-Scale Structure, [JCAP **06** \(2020\) 001](#), [[1909.07951](#)].
- [6] PLANCK collaboration, N. Aghanim et al., Planck 2018 results. VI. Cosmological parameters, [Astron. Astrophys. **641** \(2020\) A6](#), [[1807.06209](#)].
- [7] P. Zhang and Y. Cai, BOSS full-shape analysis from the EFTofLSS with exact time dependence, [Journal of Cosmology and Astroparticle Physics **2022** \(jan, 2022\) 031](#).
- [8] P. Carrilho, C. Moretti and A. Pourtsidou, Cosmology with the EFTofLSS and BOSS: dark energy constraints and a note on priors, [Journal of Cosmology and Astroparticle Physics **2023** \(jan, 2023\) 028](#).
- [9] P. Zhang, G. D’Amico, L. Senatore, C. Zhao and Y. Cai, BOSS Correlation Function Analysis from the Effective Field Theory of Large-Scale Structure, [2110.07539](#).
- [10] S.-F. Chen, Z. Vlah and M. White, A new analysis of the BOSS survey, including full-shape information and post-reconstruction BAO, [2110.05530](#).
- [11] T. Simon, P. Zhang and V. Poulin, Cosmological inference from the EFTofLSS: the eBOSS QSO full-shape analysis, [2210.14931](#).
- [12] O. H. E. Philcox and M. M. Ivanov, The BOSS DR12 Full-Shape Cosmology: Λ CDM Constraints from the Large-Scale Galaxy Power Spectrum and Bispectrum, [2112.04515](#).
- [13] M. Tsedrik, C. Moretti, P. Carrilho, F. Rizzo and A. Pourtsidou, Interacting dark energy from the joint analysis of the power spectrum and bispectrum multipoles with the EFTofLSS, [Monthly Notices of the Royal Astronomical Society **520** \(jan, 2023\) 2611–2632](#).
- [14] G. D’Amico, Y. Donath, M. Lewandowski, L. Senatore and P. Zhang, The boss bispectrum analysis at one loop from the effective field theory of large-scale structure, 2022.

- [15] O. H. Philcox, M. M. Ivanov, G. Cabass, M. Simonović, M. Zaldarriaga and T. Nishimichi, Cosmology with the redshift-space galaxy bispectrum monopole at one-loop order, [*Physical Review D* **106** \(aug, 2022\)](#) .
- [16] M. M. Ivanov, O. H. Philcox, G. Cabass, T. Nishimichi, M. Simonović and M. Zaldarriaga, Cosmology with the galaxy bispectrum multipoles: Optimal estimation and application to BOSS data, [*Physical Review D* **107** \(apr, 2023\)](#) .
- [17] O. H. E. Philcox, M. M. Ivanov, M. Simonović and M. Zaldarriaga, Combining Full-Shape and BAO Analyses of Galaxy Power Spectra: A 1.6\% CMB-independent constraint on H_0 , [*JCAP* **05** \(2020\) 032](#), [2002.04035].
- [18] G. D’Amico, L. Senatore and P. Zhang, Limits on w CDM from the EFTofLSS with the PyBird code, [*JCAP* **01** \(2021\) 006](#), [2003.07956].
- [19] G. D’Amico, Y. Donath, L. Senatore and P. Zhang, Limits on Clustering and Smooth Quintessence from the EFTofLSS, [2012.07554](#).
- [20] A. G. Riess, S. Casertano, W. Yuan, L. M. Macri and D. Scolnic, Large Magellanic Cloud Cepheid Standards Provide a 1% Foundation for the Determination of the Hubble Constant [*Astrophys. J.* **876** \(2019\) 85](#), [1903.07603].
- [21] W. L. Freedman et al., The Carnegie-Chicago Hubble Program. VIII. An Independent Determination of the Hubble Constant Based on the T [1907.05922](#).
- [22] L. Verde, T. Treu and A. G. Riess, Tensions between the Early and the Late Universe, in *Nature Astronomy* 2019, 2019. [1907.10625](#). DOI.
- [23] G. D’Amico, L. Senatore, P. Zhang and H. Zheng, The Hubble Tension in Light of the Full-Shape Analysis of Large-Scale Structure Data, [*JCAP* **05** \(2021\) 072](#), [2006.12420].
- [24] M. M. Ivanov, E. McDonough, J. C. Hill, M. Simonović, M. W. Toomey, S. Alexander et al., Constraining Early Dark Energy with Large-Scale Structure, [*Phys. Rev. D* **102** \(2020\) 103502](#), [2006.11235].
- [25] F. Niedermann and M. S. Sloth, New Early Dark Energy is compatible with current LSS data, [*Phys. Rev. D* **103** \(2021\) 103537](#), [2009.00006].
- [26] T. L. Smith, V. Poulin, J. L. Bernal, K. K. Boddy, M. Kamionkowski and R. Murgia, Early dark energy is not excluded by current large-scale structure data, [*Phys. Rev. D* **103** \(2021\) 123542](#), [2009.10740].
- [27] T. Simon, P. Zhang, V. Poulin and T. L. Smith, Updated constraints from the effective field theory analysis of BOSS power spectrum on Early Dark Energy, [2208.05930](#).
- [28] G. D’Amico, M. Lewandowski, L. Senatore and P. Zhang, Limits on primordial non-Gaussianities from BOSS galaxy-clustering data, [2201.11518](#).

- [29] G. Cabass, M. M. Ivanov, O. H. E. Philcox, M. Simonović and M. Zaldarriaga, Constraints on Single-Field Inflation from the BOSS Galaxy Survey, [*Phys. Rev. Lett.* **129** \(2022\) 021301](#), [[2201.07238](#)].
- [30] C. Moretti, M. Tsedrik, P. Carrilho and A. Pourtsidou, Modified gravity and massive neutrinos: constraints from the full shape analysis of BOSS galaxies and forecasts for S8, [*JCAP* **01** \(2023\) 034](#), [[2209.03974](#)].
- [31] T. Simon, Constraining decaying dark matter with the effective field theory of large-scale structure, in *33rd Rencontres de Blois: Exploring the Dark Universe*, 12, 2022. [2212.03004](#).
- [32] L. Piga, M. Marinucci, G. D’Amico, M. Pietroni, F. Vernizzi and B. S. Wright, Constraints on modified gravity from the BOSS galaxy survey, [*JCAP* **04** \(2023\) 038](#), [[2211.12523](#)].
- [33] A. Chudaykin, K. Dolgikh and M. M. Ivanov, Constraints on the curvature of the Universe and dynamical dark energy from the Full-shape and BAO data, [*Phys. Rev. D* **103** \(2021\) 023507](#), [[2009.10106](#)].
- [34] G. Cabass, M. M. Ivanov, O. H. E. Philcox, M. Simonović and M. Zaldarriaga, Constraints on multifield inflation from the BOSS galaxy survey, [*Phys. Rev. D* **106** \(2022\) 043506](#), [[2204.01781](#)].
- [35] A. Semenaite, A. G. Sánchez, A. Pezzotta, J. Hou, A. Eggemeier, M. Crocce et al., Beyond Λ CDM constraints from the full shape clustering measurements from BOSS and eBOSS, [*Mon. Not. Roy. Astron. Soc.* **521** \(2023\) 5013–5025](#), [[2210.07304](#)].
- [36] H. Rubira, A. Mazoun and M. Garny, Full-shape BOSS constraints on dark matter interacting with dark radiation and lifting the S8 tension, [*JCAP* **01** \(2023\) 034](#), [[2209.03974](#)].
- [37] P. Carrilho, C. Moretti and A. Pourtsidou, Cosmology with the EFTofLSS and BOSS: dark energy constraints and a note on priors, [*JCAP* **01** \(2023\) 028](#), [[2207.14784](#)].
- [38] T. Simon, G. Franco Abellán, P. Du, V. Poulin and Y. Tsai, Constraining decaying dark matter with BOSS data and the effective field theory of large-scale structures, [*Phys. Rev. D* **106** \(2022\) 023516](#), [[2203.07440](#)].
- [39] R. A. Porto, L. Senatore and M. Zaldarriaga, The Lagrangian-space Effective Field Theory of Large Scale Structures, [*JCAP* **1405** \(2014\) 022](#), [[1311.2168](#)].
- [40] J. J. M. Carrasco, S. Foreman, D. Green and L. Senatore, The 2-loop matter power spectrum and the IR-safe integrand, [*JCAP* **1407** \(2014\) 056](#), [[1304.4946](#)].
- [41] J. J. M. Carrasco, S. Foreman, D. Green and L. Senatore, The Effective Field Theory of Large Scale Structures at Two Loops, [*JCAP* **1407** \(2014\) 057](#), [[1310.0464](#)].
- [42] S. M. Carroll, S. Leichenauer and J. Pollack, Consistent effective theory of long-wavelength cosmological perturbations, [*Phys. Rev.* **D90** \(2014\) 023518](#), [[1310.2920](#)].

- [43] L. Senatore and M. Zaldarriaga, The IR-resummed Effective Field Theory of Large Scale Structures, [JCAP **1502** \(2015\) 013](#), [[1404.5954](#)].
- [44] T. Baldauf, E. Schaan and M. Zaldarriaga, On the reach of perturbative methods for dark matter density fields, [JCAP **1603** \(2016\) 007](#), [[1507.02255](#)].
- [45] S. Foreman, H. Perrier and L. Senatore, Precision Comparison of the Power Spectrum in the EFTofLSS with Simulations, [JCAP **1605** \(2016\) 027](#), [[1507.05326](#)].
- [46] T. Baldauf, L. Mercolli and M. Zaldarriaga, Effective field theory of large scale structure at two loops: The apparent scale dependence of the speed of sound, [Phys. Rev. **D92** \(2015\) 123007](#), [[1507.02256](#)].
- [47] M. Cataneo, S. Foreman and L. Senatore, Efficient exploration of cosmology dependence in the EFT of LSS, [1606.03633](#).
- [48] M. Lewandowski and L. Senatore, IR-safe and UV-safe integrands in the EFTofLSS with exact time dependence, [JCAP **1708** \(2017\) 037](#), [[1701.07012](#)].
- [49] T. Konstandin, R. A. Porto and H. Rubira, The Effective Field Theory of Large Scale Structure at Three Loops, [1906.00997](#).
- [50] E. Pajer and M. Zaldarriaga, On the Renormalization of the Effective Field Theory of Large Scale Structures, [JCAP **1308** \(2013\) 037](#), [[1301.7182](#)].
- [51] A. A. Abolhasani, M. Mirbabayi and E. Pajer, Systematic Renormalization of the Effective Theory of Large Scale Structure, [JCAP **1605** \(2016\) 063](#), [[1509.07886](#)].
- [52] L. Mercolli and E. Pajer, On the velocity in the Effective Field Theory of Large Scale Structures, [JCAP **1403** \(2014\) 006](#), [[1307.3220](#)].
- [53] M. McQuinn and M. White, Cosmological perturbation theory in 1+1 dimensions, [JCAP **1601** \(2016\) 043](#), [[1502.07389](#)].
- [54] L. Senatore, Bias in the Effective Field Theory of Large Scale Structures, [JCAP **1511** \(2015\) 007](#), [[1406.7843](#)].
- [55] L. Senatore and M. Zaldarriaga, Redshift Space Distortions in the Effective Field Theory of Large Scale Structures, [1409.1225](#).
- [56] T. Baldauf, M. Mirbabayi, M. Simonovic and M. Zaldarriaga, Equivalence Principle and the Baryon Acoustic Peak, [Phys. Rev. **D92** \(2015\) 043514](#), [[1504.04366](#)].
- [57] L. Senatore and G. Trevisan, On the IR-Resummation in the EFTofLSS, [JCAP **1805** \(2018\) 019](#), [[1710.02178](#)].
- [58] M. Lewandowski and L. Senatore, An analytic implementation of the IR-resummation for the BAO peak, [1810.11855](#).

- [59] D. Blas, M. Garny, M. M. Ivanov and S. Sibiryakov,
Time-Sliced Perturbation Theory II: Baryon Acoustic Oscillations and Infrared Resummation,
[JCAP 1607 \(2016\) 028](#), [[1605.02149](#)].
- [60] M. Lewandowski, A. Perko and L. Senatore,
Analytic Prediction of Baryonic Effects from the EFT of Large Scale Structures, [JCAP 1505 \(2015\) 019](#), [[1412.5049](#)].
- [61] D. P. L. Bragança, M. Lewandowski, D. Sekera, L. Senatore and R. Sgier,
Baryonic effects in the Effective Field Theory of Large-Scale Structure and an analytic recipe for lensing in CMB-S4,
[2010.02929](#).
- [62] R. E. Angulo, S. Foreman, M. Schmittfull and L. Senatore,
The One-Loop Matter Bispectrum in the Effective Field Theory of Large Scale Structures, [JCAP 1510 \(2015\) 039](#), [[1406.4143](#)].
- [63] T. Baldauf, L. Mercolli, M. Mirbabayi and E. Pajer,
The Bispectrum in the Effective Field Theory of Large Scale Structure, [JCAP 1505 \(2015\) 007](#), [[1406.4135](#)].
- [64] D. Bertolini, K. Schutz, M. P. Solon and K. M. Zurek,
The Trispectrum in the Effective Field Theory of Large Scale Structure, [1604.01770](#).
- [65] T. Baldauf, E. Schaan and M. Zaldarriaga,
On the reach of perturbative descriptions for dark matter displacement fields, [JCAP 1603 \(2016\) 017](#), [[1505.07098](#)].
- [66] S. Foreman and L. Senatore,
The EFT of Large Scale Structures at All Redshifts: Analytical Predictions for Lensing, [JCAP 1604 \(2016\) 033](#), [[1503.01775](#)].
- [67] M. Mirbabayi, F. Schmidt and M. Zaldarriaga, Biased Tracers and Time Evolution, [JCAP 1507 \(2015\) 030](#), [[1412.5169](#)].
- [68] R. Angulo, M. Fasiello, L. Senatore and Z. Vlah,
On the Statistics of Biased Tracers in the Effective Field Theory of Large Scale Structures, [JCAP 1509 \(2015\) 029](#), [[1503.08826](#)].
- [69] T. Fujita, V. Mauerhofer, L. Senatore, Z. Vlah and R. Angulo,
Very Massive Tracers and Higher Derivative Biases, [1609.00717](#).
- [70] A. Perko, L. Senatore, E. Jennings and R. H. Wechsler,
Biased Tracers in Redshift Space in the EFT of Large-Scale Structure, [1610.09321](#).
- [71] E. O. Nadler, A. Perko and L. Senatore,
On the Bispectra of Very Massive Tracers in the Effective Field Theory of Large-Scale Structure,
[JCAP 1802 \(2018\) 058](#), [[1710.10308](#)].
- [72] Y. Donath and L. Senatore,
Biased Tracers in Redshift Space in the EFTofLSS with exact time dependence, [JCAP 10 \(2020\) 039](#), [[2005.04805](#)].

- [73] P. McDonald and A. Roy, Clustering of dark matter tracers: generalizing bias for the coming era of precision LSS, [JCAP](#) **0908** (2009) 020, [[0902.0991](#)].
- [74] M. Lewandowski, L. Senatore, F. Prada, C. Zhao and C.-H. Chuang, EFT of large scale structures in redshift space, [Phys. Rev.](#) **D97** (2018) 063526, [[1512.06831](#)].
- [75] L. Senatore and M. Zaldarriaga, The Effective Field Theory of Large-Scale Structure in the presence of Massive Neutrinos, [1707.04698](#).
- [76] R. de Belsunce and L. Senatore, Tree-Level Bispectrum in the Effective Field Theory of Large-Scale Structure extended to Massive Neutrinos, [1804.06849](#).
- [77] M. Lewandowski, A. Maleknejad and L. Senatore, An effective description of dark matter and dark energy in the mildly non-linear regime, [JCAP](#) **1705** (2017) 038, [[1611.07966](#)].
- [78] G. Cusin, M. Lewandowski and F. Vernizzi, Dark Energy and Modified Gravity in the Effective Field Theory of Large-Scale Structure, [JCAP](#) **1804** (2018) 005, [[1712.02783](#)].
- [79] B. Bose, K. Koyama, M. Lewandowski, F. Vernizzi and H. A. Winther, Towards Precision Constraints on Gravity with the Effective Field Theory of Large-Scale Structure, [JCAP](#) **1804** (2018) 063, [[1802.01566](#)].
- [80] V. Assassi, D. Baumann, E. Pajer, Y. Welling and D. van der Woude, Effective theory of large-scale structure with primordial non-Gaussianity, [JCAP](#) **1511** (2015) 024, [[1505.06668](#)].
- [81] V. Assassi, D. Baumann and F. Schmidt, Galaxy Bias and Primordial Non-Gaussianity, [JCAP](#) **1512** (2015) 043, [[1510.03723](#)].
- [82] D. Bertolini, K. Schutz, M. P. Solon, J. R. Walsh and K. M. Zurek, Non-Gaussian Covariance of the Matter Power Spectrum in the Effective Field Theory of Large Scale Structure, [1512.07630](#).
- [83] D. Bertolini and M. P. Solon, Principal Shapes and Squeezed Limits in the Effective Field Theory of Large Scale Structure, [1608.01310](#).
- [84] M. Simonovic, T. Baldauf, M. Zaldarriaga, J. J. Carrasco and J. A. Kollmeier, Cosmological perturbation theory using the FFTLog: formalism and connection to QFT loop integrals, [JCAP](#) **1804** (2018) 030, [[1708.08130](#)].
- [85] T. Nishimichi, G. D'Amico, M. M. Ivanov, L. Senatore, M. Simonović, M. Takada et al., Blinded challenge for precision cosmology with large-scale structure: results from effective field theory for the redshift, [Phys. Rev. D](#) **102** (2020) 123541, [[2003.08277](#)].
- [86] S.-F. Chen, Z. Vlah, E. Castorina and M. White, Redshift-Space Distortions in Lagrangian Perturbation Theory, [JCAP](#) **03** (2021) 100, [[2012.04636](#)].

- [87] BOSS collaboration, S. Alam et al.,
The clustering of galaxies in the completed SDSS-III Baryon Oscillation Spectroscopic Survey: cosmological analysis of the SDSS-III Baryon Oscillation Spectroscopic Survey,
[Mon. Not. Roy. Astron. Soc.](#) **470** (2017) 2617–2652, [[1607.03155](#)].
- [88] DESI collaboration, A. Aghamousa et al.,
The DESI Experiment Part I: Science, Targeting, and Survey Design, [1611.00036](#).
- [89] D. J. Schlegel et al.,
The MegaMapper: A Stage-5 Spectroscopic Instrument Concept for the Study of Inflation and Dark Energy,
[2209.04322](#).
- [90] D. J. H. Chung, M. Münchmeyer and S. C. Tadepalli,
Search for Isocurvature with Large-scale Structure: A Forecast for Euclid and MegaMapper using EFTofLSS,
[2306.09456](#).
- [91] T. Kajita, Nobel Lecture: Discovery of atmospheric neutrino oscillations, [Rev. Mod. Phys.](#) **88** (2016) 030501.
- [92] R. Bousso, D. Harlow and L. Senatore, Inflation after False Vacuum Decay: observational Prospects after Planck, [Phys. Rev. D](#) **91** (2015) 083527, [[1309.4060](#)].
- [93] M. Kleban and M. Schillo, Spatial Curvature Falsifies Eternal Inflation, [JCAP](#) **06** (2012) 029, [[1202.5037](#)].
- [94] D. Babich, P. Creminelli and M. Zaldarriaga, The Shape of non-Gaussianities, [JCAP](#) **08** (2004) 009, [[astro-ph/0405356](#)].
- [95] P. Creminelli, A. Nicolis, L. Senatore, M. Tegmark and M. Zaldarriaga,
Limits on non-gaussianities from wmap data, [JCAP](#) **0605** (2006) 004, [[astro-ph/0509029](#)].
- [96] L. Senatore, K. M. Smith and M. Zaldarriaga,
Non-Gaussianities in Single Field Inflation and their Optimal Limits from the WMAP 5-year Data,
[JCAP](#) **1001** (2010) 028, [[0905.3746](#)].
- [97] C. Cheung, P. Creminelli, A. L. Fitzpatrick, J. Kaplan and L. Senatore,
The Effective Field Theory of Inflation, [JHEP](#) **03** (2008) 014, [[0709.0293](#)].
- [98] F. Bernardeau and J.-P. Uzan, NonGaussianity in multifield inflation, [Phys. Rev. D](#) **66** (2002) 103506, [[hep-ph/0207295](#)].
- [99] D. H. Lyth, C. Ungarelli and D. Wands,
The Primordial density perturbation in the curvaton scenario, [Phys. Rev. D](#) **67** (2003) 023503, [[astro-ph/0208055](#)].
- [100] M. Zaldarriaga, Non-Gaussianities in models with a varying inflaton decay rate, [Phys. Rev. D](#) **69** (2004) 043508, [[astro-ph/0306006](#)].
- [101] L. Senatore and M. Zaldarriaga, The Effective Field Theory of Multifield Inflation, [JHEP](#) **04** (2012) 024, [[1009.2093](#)].
- [102] G. Cabass, M. M. Ivanov, O. H. E. Philcox, M. Simonovic and M. Zaldarriaga,
Constraining single-field inflation with MegaMapper, [Phys. Lett. B](#) **841** (2023) 137912, [[2211.14899](#)].

- [103] R. Flauger, M. Mirbabayi, L. Senatore and E. Silverstein, Productive Interactions: heavy particles and non-Gaussianity, [JCAP](#) **10** (2017) 058, [[1606.00513](#)].
- [104] C. Anastasiou, D. P. L. Bragança, L. Senatore and H. Zheng, Efficiently evaluating loop integrals in the EFTofLSS using QFT integrals with massive propagators, [2212.07421](#).
- [105] PLANCK collaboration, Y. Akrami et al., Planck 2018 results. IX. Constraints on primordial non-Gaussianity, [Astron. Astrophys.](#) **641** (2020) A9, [[1905.05697](#)].
- [106] M. Tegmark, Measuring cosmological parameters with galaxy surveys, [Phys. Rev. Lett.](#) **79** (1997) 3806–3809, [[astro-ph/9706198](#)].
- [107] N. Agarwal, V. Desjacques, D. Jeong and F. Schmidt, Information content in the redshift-space galaxy power spectrum and bispectrum, [JCAP](#) **03** (2021) 021, [[2007.04340](#)].
- [108] V. Yankelevich and C. Porciani, Cosmological information in the redshift-space bispectrum, [Mon. Not. Roy. Astron. Soc.](#) **483** (2019) 2078–2099, [[1807.07076](#)].
- [109] D. Baumann, D. Green and B. Wallisch, Searching for light relics with large-scale structure, [JCAP](#) **08** (2018) 029, [[1712.08067](#)].
- [110] G. D’Amico, Y. Donath, M. Lewandowski, L. Senatore and P. Zhang, The BOSS bispectrum analysis at one loop from the Effective Field Theory of Large-Scale Structure, [2206.08327](#).
- [111] G. D’Amico, Y. Donath, M. Lewandowski, L. Senatore and P. Zhang, The one-loop bispectrum of galaxies in redshift space from the Effective Field Theory of Large-Scale Structure, [2211.17130](#).
- [112] H. A. Feldman, N. Kaiser and J. A. Peacock, Power spectrum analysis of three-dimensional redshift surveys, [Astrophys. J.](#) **426** (1994) 23–37, [[astro-ph/9304022](#)].
- [113] R. Scoccimarro, S. Colombi, J. N. Fry, J. A. Frieman, E. Hivon and A. Melott, Nonlinear evolution of the bispectrum of cosmological perturbations, [Astrophys. J.](#) **496** (1998) 586, [[astro-ph/9704075](#)].
- [114] K. C. Chan and L. Blot, Assessment of the Information Content of the Power Spectrum and Bispectrum, [Phys. Rev. D](#) **96** (2017) 023528, [[1610.06585](#)].
- [115] E. Sefusatti, M. Crocce, S. Pueblas and R. Scoccimarro, Cosmology and the Bispectrum, [Phys. Rev. D](#) **74** (2006) 023522, [[astro-ph/0604505](#)].
- [116] V. Desjacques, D. Jeong and F. Schmidt, Large-Scale Galaxy Bias, [Phys. Rept.](#) **733** (2018) 1–193, [[1611.09787](#)].
- [117] S. Ferraro et al., Inflation and Dark Energy from Spectroscopy at $z > 2$, [Bull. Am. Astron. Soc.](#) **51** (2019) 72, [[1903.09208](#)].

- [118] N. Kokron, J. DeRose, S.-F. Chen, M. White and R. H. Wechsler,
Priors on red galaxy stochasticity from hybrid effective field theory, [Mon. Not. Roy. Astron. Soc.](#)
514 (2022) 2198–2213, [[2112.00012](#)].
- [119] C. Alcock and B. Paczynski, An evolution free test for non-zero cosmological constant, [Nature](#) **281**
(1979) 358–359.
- [120] T. Baldauf, U. Seljak and L. Senatore,
Primordial non-Gaussianity in the Bispectrum of the Halo Density Field, [JCAP](#) **04** (2011) 006,
[[1011.1513](#)].
- [121] Y. Donath and L. Senatore, Exact Trispectrum covariances and Fisher matrices, [in progress](#).
- [122] T. Steele and T. Baldauf,
Precise Calibration of the One-Loop Trispectrum in the Effective Field Theory of Large Scale Structure,
[Phys. Rev. D](#) **103** (2021) 103518, [[2101.10289](#)].
- [123] B. Reid et al.,
SDSS-III Baryon Oscillation Spectroscopic Survey Data Release 12: galaxy target selection and large scale structure
[Mon. Not. Roy. Astron. Soc.](#) **455** (2016) 1553–1573, [[1509.06529](#)].
- [124] BOSS collaboration, F. Beutler et al.,
The clustering of galaxies in the completed SDSS-III Baryon Oscillation Spectroscopic Survey: Anisotropic galaxy clustering
[Mon. Not. Roy. Astron. Soc.](#) **466** (2017) 2242–2260, [[1607.03150](#)].
- [125] A. Font-Ribera, P. McDonald, N. Mostek, B. A. Reid, H.-J. Seo and A. Slosar,
DESI and other dark energy experiments in the era of neutrino mass measurements, [JCAP](#) **05**
(2014) 023, [[1308.4164](#)].